Mixing characteristics of an inhomogeneous scalar in isotropic and homogeneous sheared turbulence

K. K. Nomura and S. E. Elghobashi
Department of Mechanical and Aerospace Engineering, University of California, Irvine, California 92717

(Received 17 October 1990; accepted 5 November 1991)

Turbulent mixing of an inhomogeneous passive scalar field is studied in the context of a nonpremixed reacting flow. Direct numerical simulations of an initial steplike scalar field subjected to homogeneous sheared turbulence have been performed and the results compared with those of the case of decaying isotropic turbulence. For both flow conditions, the gradient of the conserved scalar tends to align itself with the axis of the most compressive strain rate and orthogonal to the local vorticity. The magnitude of the scalar gradient is directly influenced by the local strain rate while its orientation is controlled by the local vorticity. Because of the directional features of sheared turbulence, the orientation of the scalar gradient is more ordered than in isotropic turbulence. In addition, the magnitude of vorticity indirectly affects that of the scalar gradient through strain-rate amplification by vortex stretching. In both flows, regions of high scalar-gradient magnitude or scalar dissipation (and therefore high reaction rates) tend to exist as sheets in the vicinity of sheetlike vortex structures of moderate to high vorticity. The probability density function (pdf) of the the scalar dissipation rate ϵ_F exhibits a nearly lognormal distribution with a slight negative skewness for both isotropic and sheared turbulence.

I. INTRODUCTION

Turbulent nonpremixed (or diffusion) flames are those in which initially separate fuel and oxidant streams react upon mixing. The reaction is predominantly mixing controlled since the time scale of chemical reaction is usually orders of magnitude smaller than the smallest time scale of turbulence. In the limit of an infinite reaction rate, the reaction is confined to an isoscalar surface of zero thickness at stoichiometric conditions. The reactants are transported toward the surface from opposite sides and instantly vanish at the surface where only product exists. In this case, the solution of a single conserved scalar is sufficient to describe the temporal and spatial distributions of the species concentration.[1,2] With negligible heat release (exothermic energy), the problem becomes that of passive scalar mixing in which the initial step profile evolves into an inhomogeneous scalar field. The turbulent motion generates small-scale fluctuations in the scalar field (scalar variance) by advection and distortion of the material elements of fluid. There is a continual reduction in the scales of the scalar fluctuations by turbulence. At the smallest scales, the scalar variance is ultimately destroyed by molecular diffusion. Mixing is then completed at the molecular level and chemical reaction can occur. The rate of molecular mixing is governed by the rate of scalar dissipation and thus, for the above conditions, controls the reaction rate. Understanding the details of turbulent scalar mixing is a prerequisite to understanding and predicting the physical processes occuring in nonpremixed flames.

Early descriptions of turbulent scalar mixing were established by the work of Obukhov[3] and Corrsin.[4] The scalar transport equation in Fourier space shows that the advective term is responsible for the transfer of scalar variance across the spectrum, hence the generation of the high wave-number components (small scales) in the scalar field. The physical mechanism by which the rate of strain field influences the scalar mixing field was first studied by Batchelor.[5] For the case of weakly diffusive scalars ($\nu \gg D$), for which the Kolmogorov microscale exceeds the scalar microscale, a locally uniform strain field is "seen" by the small-scale scalar fluctuations. The effect of convection on the scalar field is nearly that of a pure straining motion. The local scalar gradient aligns with the principal axis of the least strain rate (compressive) and is amplified under the compressive action. The effect of diffusion is to counteract this amplification and erase the inhomogeneities in the scalar field.

The significance of the local strain rate in generating small-scale scalar fluctuations was further elucidated by Gibson.[6,7] Gibson proposed two mixing mechanisms involving the interaction of the local strain with minimal and maximal scalar-gradient lines. In the first mechanism,[6] extrema in the scalar field are generated by turbulent eddies with secondary generation by pinching and splitting in the direction of the local stretching strain. These regions are connected by lines of minimal scalar gradient that tend to move with the fluid and thus have time to be influenced by the local rate of strain. The second mechanism[7] involves the creation of maximal gradient lines due to the alignment of the local scalar gradient with the compressive strain axes. This results in the amplification of the local scalar gradient, which tends to decrease the diffusion velocity and causes further amplification through a positive feedback process. Since the strain axes are orthogonal, the two mechanisms tend to act orthogonal to each other. The influence of the local strain rate is assumed to occur over distances much greater than the Kolmogorov microscale η, in contrast to the earlier description given by Batchelor.[5]

Recently, results from direct numerical simulations

 0899-8213/92/030606-20$04.00

(DNS) have provided much insight into the small-scale structure of turbulence and mechanisms of scalar mixing. Kerr[8] performed direct simulations of stationary (forced) isotropic turbulence with a forced isotropic scalar field and, from graphical display, found distinct alignment characteristics between the vorticity, strain rate, and scalar-gradient fields. Vorticity appears to be concentrated in tubes with the scalar gradient and most compressive strain aligned perpendicular to the tubes. High-magnitude scalar gradient occurs as sheets that wrap around the vortex tubes, however, the magnitude of the scalar gradient was found to be uncorrelated with that of the vorticity. Ashurst *et al.*[9] obtained additional statistics from the direct simulation results of Kerr[8] and from those of Rogers and Moin[10] for a homogeneous shear flow with a uniform scalar gradient. Alignment probabilities of the vorticity and scalar gradient with the principal strain-rate directions were presented. Their results were consistent with those of Kerr's and suggested that turbulence is characterized by the presence of stretching vortex structures that exhibit distinct alignment with the strain axes. Alignment characteristics of the scalar showed that the scalar gradient tends to align with the most compressive strain axes and normal to the vorticity suggesting amplification of the scalar gradient by both rotation and compressive straining. More recently, She *et al.*[11] and Ruetsch and Maxey[12] found, based on simulations of homogeneous isotropic turbulence, that regions of intense vorticity exist as tubelike structures and regions of moderate vorticity exist as sheetlike structures. Regions of moderate to high scalar gradient were found to wrap around the tubelike vortex structures, however, regions of the highest scalar gradient exist as sheets and occur near the vortex sheets rather than the tubes.[12]

The above studies considered homogeneous velocity and scalar fields. As mentioned earlier, a nonpremixed reaction involves an *inhomogeneous* scalar field as a result of the initially separate reactant streams. Direct simulations of a nonpremixed reaction in decaying isotropic turbulence were performed by Leonard and Hill.[13] Direct simulations of a nonpremixed reaction in both decaying isotropic turbulence and homogeneous shear flow have been performed by Nomura and Elghobashi,[14] Elghobashi and Nomura,[15] and Leonard and Hill.[16] The studies by Leonard and Hill[13,16] included the effects of both finite and infinite chemical reaction rate. As in the inert case, the reactant concentration gradients were found to align with the direction of the most compressive strain. Results indicate that high reaction rates occur in regions where the alignment is strong and the local strain rate is high. Although the case of shear flow was investigated, the emphasis of their study was on the unsheared condition.

The objective of the present work is to further study the basic mechanisms of turbulent mixing in an inhomogeneous scalar field characteristic of a two-stream nonpremixed reaction using direct numerical simulation. Since no modeling is used in direct simulations, the small-scale structure of the flow is captured, thus revealing the underlying physics of the turbulent mixing processes. The limiting case of an infinitely fast reaction rate is assumed so that the reaction is controlled entirely by mixing. The scalar is passive and thus does not affect the velocity field. Two basic flow conditions are considered: decaying isotropic turbulence, in which strain rates decrease in time, and homogeneous shear flow, in which strain rates tend to increase in time. The influence of the strain rate and vorticity fields and the presence of mean shear on the scalar mixing process are investigated.

II. MATHEMATICAL DESCRIPTION

A. Flow description and computational domain

The chemical reaction considered in this study is an isothermal reaction between two species diluted in an inert gas, such that the density of the fluid remains constant throughout the flow. The scalar and velocity fields are therefore uncoupled, i.e., the scalar is passive. Both fuel and oxidant have equal Schmidt numbers ($\mathrm{Sc} = \nu/D = 0.7$), and the binary chemical reaction proceeds to completion in a single step with a fixed stoichiometric ratio to form the product. These assumptions allow a linear combination of the equations describing the conservation of the two nonpremixed reactants (fuel and oxidant) to yield an equation for a conserved scalar,[1,2] denoted here by the mixture fraction. The mixture fraction F is defined by $F \equiv (\beta - \beta_2)/(\beta_1 - \beta_2)$, where β is a Shvab–Zeldovich variable and $\beta \equiv m_{\mathrm{fu}} - m_{\mathrm{ox}}/r$, where m_{fu} and m_{ox} are the mass fractions of fuel and oxidant. The quantity r is the mass of oxidant per unit mass of fuel required for complete reaction. The subscripts 1 and 2 denote the two initial homogeneous reactant streams. In the limit of an infinite reaction rate, the reaction will be confined to a surface at which stoichiometric conditions exist ($F = F_{\mathrm{st}}$) at any instant of time. Knowledge of the conserved scalar F determines the entire composition of the fluid.

Both homogeneous shear flow and decaying isotropic grid turbulence are considered. Figure 1 shows the mean velocity profile $U(z)$ associated with a uniform mean shear in the z direction and the initial step profile of the mixture fraction $F(z,t_0)$ representing the two-reactant stream system. Our computational domain is a finite cube with sides of length L, containing 128^3 grid points. Initially, fuel ($F = 1$)

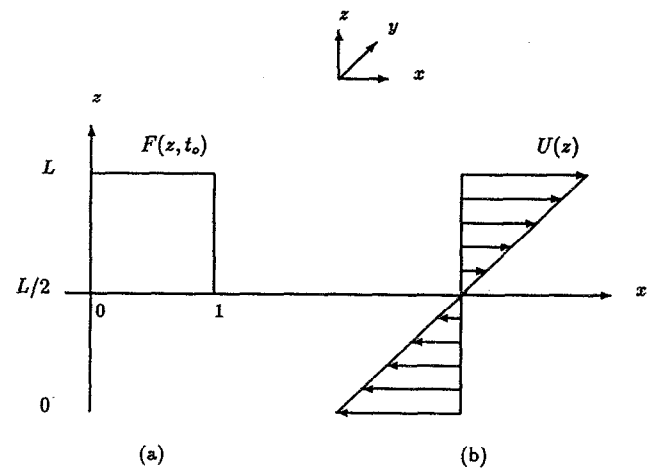

FIG. 1. Flow representation: (a) initial profile of the mixture fraction $F(z,t_0)$, (b) mean velocity $U(z)$.

is admitted into the upper half of the domain and oxidant ($F=0$) into the lower half.

B. Governing equations

The governing equations are the instantaneous, three-dimensional Navier–Stokes, scalar (mixture fraction) conservation and continuity equations, which can be written as

$$\frac{\partial u_i}{\partial t}+\frac{\partial}{\partial x_j}(u_j u_i)+Sx_3\frac{\partial u_i}{\partial x_1}+Su_3\delta_{i1} =\frac{1}{\mathrm{Re}}\frac{\partial^2 u_i}{\partial x_j^2}-\frac{\partial p}{\partial x_i}, \tag{1}$$

$$\frac{\partial f}{\partial t}+\frac{\partial}{\partial x_j}(u_j f)+Sx_3\frac{\partial f}{\partial x_1}+su_3=\frac{1}{\mathrm{Re\,Sc}}\frac{\partial^2 f}{\partial x_j^2}, \tag{2}$$

$$\frac{\partial u_j}{\partial x_j}=0, \tag{3}$$

in which Cartesian tensor notation is employed and $i=1,2,3$ corresponds to the x,y,z directions (Fig. 1). In the above equations, u_i, f, and p are the deviations of the instantaneous velocity, mixture fraction, and pressure from their respective reference profiles. For example,

$$f(x,y,z,t)=F(x,y,z,t)-F_{\mathrm{ref}}(z), \tag{4}$$

where $F_{\mathrm{ref}}(z)=z(dF/dz)_{\mathrm{ref}}$ and $(dF/dz)_{\mathrm{ref}}$ is a fixed reference gradient for the mixture fraction.[17] By subtracting a fixed reference or mean value from the computed field variables, widely disparate values are avoided thus improving the accuracy of the computation. The nondimensional shear S and the nondimensional mixture fraction gradient s are defined as $S=(L/\Delta U)(dU/dz)_{\mathrm{ref}}$, and $s=(L/\Delta F)(dF/dz)_{\mathrm{ref}}$, where ΔU and ΔF are the differences in the mean velocity and mixture fraction at the top and bottom of the computational domain. Reference values are defined such that $S=1$ and $s=1$. The characteristic quantities used in the nondimensionalization of Eqs. (1)–(3) are L, ΔU, ΔF, and a reference density ρ_0. Time is therefore nondimensionalized by $L/\Delta U$. In the case of isotropic (nonsheared) turbulence, $S=0$, and time is scaled by L/U, where U is the reference uniform free-stream velocity.

In the case of homogeneous shear, the reference profile $U(z)$ coincides with the mean velocity profile, thus the computed deviations $u_i(x,y,z,t)$ are the velocity fluctuations. However, since the scalar reference profile $F_{\mathrm{ref}}(z)$ does not coincide with the mean scalar profile $\overline{F}(z,t)$ that develops in time, local instantaneous fluctuations of the mixture fraction are evaluated from

$$f'(x,y,z,t)=F(x,y,z,t)-\overline{F}(z,t), \tag{5}$$

where $\overline{F}(z,t)=\langle F(x,y,z,t)\rangle_{x,y}$ is the ensemble-averaged mixture fraction over a horizontal (x-y) plane.

C. Initial and boundary conditions

The simulations are initialized with velocity fields that are divergence free and have random fluctuations prescribed by an appropriate three-dimensional energy spectrum $E(k,0)$. For the isotropic flows, the following spectrum function is used:

$$E(k,0)=(3v_0^2/2)(k/k_p^2)e^{-(k/k_p)}, \tag{6}$$

where k_p is the wave number of the spectrum peak and v_0 is the initial rms velocity $[v_0=(\langle u_i u_i\rangle/3)^{1/2}]$. This spectrum function is associated with the initial period of decay for isotropic turbulence,[18] which is characterized by a relatively higher energy content at the lower wave numbers. The initial value of k_p is set equal to $6(2\pi)$ for the present simulations, where the highest wave number equals $64(2\pi)$. The suitability of the initial flow field was tested for isotropic flows by monitoring the decay rate of $E(k,t)$ and the time development of the skewness of the velocity derivative and the anisotropy tensor $(b_{ij}=\langle u_i u_j\rangle/\langle u_k u_k\rangle-1/3\delta_{ij})$, for which the diagonal components b_{ii} should remain relatively equal and small in magnitude under conditions of isotropy. For shear flows, an alternative spectrum function is used:

$$E(k,0)=16\left(\frac{2}{\pi}\right)^{1/2}\left(\frac{3v_0^2}{2}\right)\left(\frac{k^4}{k_p^5}\right)e^{-2(k/k_p)^2}, \tag{7}$$

where the selected initial value of k_p is $8(2\pi)$. This function produces a narrower spectrum than that of (6) with most of the energy content confined in wave numbers surrounding k_p, i.e., not the lowest wave numbers. This serves to reduce the size of the initial integral length scale, thus extending the duration of the shear flow simulations without violating the assumption of periodic boundary conditions in the streamwise direction.

The characteristic length scales of the flow are the integral length scale

$$\ell=\frac{1}{2v^2}\int\frac{E(k)}{k}\,dk, \tag{8}$$

the Taylor microscale

$$\lambda=\sqrt{15v^2\nu/\epsilon}, \tag{9}$$

and the Kolmogorov microscale

$$\eta=(\nu^3/\epsilon)^{1/4}, \tag{10}$$

where v is the rms velocity, ϵ is the energy dissipation rate, and ν is the kinematic viscosity. The shape of the spectrum $E(k,0)$ determines the initial integral length scale ℓ_0. The value of the initial rms velocity v_0 is chosen to prescribe the initial strain number St_0 defined as

$$\mathrm{St}_0=(v_0/\ell_0)/S, \tag{11}$$

which is the ratio of the strain rate of the energy-containing eddies (large-scale strain rate) to that of the mean flow. The spectrum of the dissipation rate of turbulence energy is calculated from $\epsilon(k,t)=2\nu k^2E(k,t)$. The computed initial dissipation spectrum $\epsilon(k,0)$ has a peak at a wave number $k_d=19(2\pi)$ in the isotropic flow and $k_d=9(2\pi)$ in the shear flow. The initial turbulent Reynolds number based on the Taylor microscale $(\mathrm{Re}_{\lambda_0}=v_0\lambda_0/\nu)$ is 25 in both flow conditions. Values for Re_λ are limited by grid resolution. A fairly low initial value is required for the case of sheared turbulence since Re_λ increases in time. Further points concerning resolution are discussed below.

The skewness of the velocity derivative, given by

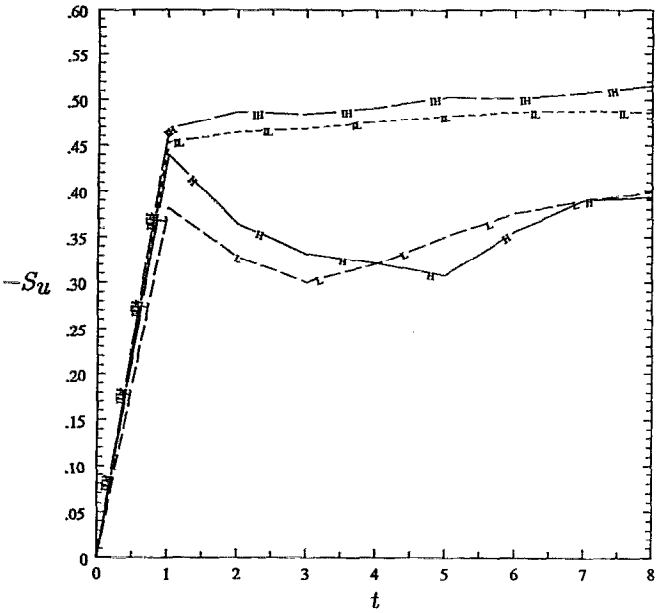

FIG. 2. Time development of the velocity derivative skewness $-S_u$ for the isotropic cases IH (— —) and IL (- - - -) and shear cases H (——) and L (– – –).

$$S_u = \sum_{i=1}^{3} \frac{\frac{1}{3}\langle(\partial u_i/\partial x_i)^3\rangle}{\{\frac{1}{3}\langle(\partial u_i/\partial x_i)^2\rangle\}^{3/2}}, \tag{12}$$

is a measure of the nonlinear energy transfer from low to high wave numbers. Computed skewness from the simulations is plotted as a function of nondimensional time in Fig. 2. The initial zero (Gaussian) value of the skewness indicates no transfer of energy. After a short period of time, it increases to its asymptotic value (≈ -0.45) in the isotropic flow case. At this time, the turbulence field is regarded as fully developed and the initial scalar (step) profile $F(z,t_0)$ is imposed.[17] The skewness takes approximately 1 unit of dimensionless time to reach a value of approximately -0.45. For the shear flow, an asymptotic state is not reached during the executed simulation time. For this case, the scalar profile is imposed after the initial rise of the total skewness ($t=1$), which indicates that the energy transfer process has been established.

The resolution in the physical space is determined by the cubical domain box size L and the number of grid points N^3. This corresponds to a minimum wave number $k_0 = 2\pi/L$ ($=2\pi$ for $L=1$ in our case) and a maximum wave number $k_{\max} = N/2 \cdot k_0 = \pi N/L$. The smallest scale captured by the simulation is therefore on the order of $1/k_{\max}$. The smallest scale of turbulence is on the order of the Kolmogorov scale η. A criterion for adequate grid resolution is therefore[19]

$$\eta k_{\max} > 1. \tag{13}$$

The initial Kolmogorov scale, normalized by L, has a value of 0.0024 for the isotropic flow and 0.0039 for the shear flow. For a resolution of $N=128$, $1/k_{\max} = 0.0025$. This gives a value of $\eta k_{\max} = 1.0$ and 1.6 for the isotropic and shear cases, respectively. Since η increases with time for decaying turbulence, the resolution is sufficient throughout the developed isotropic flow. In shear flows, ϵ tends to increase and thus η ultimately decreases in time. For the shear flow simulations presented here, the criterion (13) is met throughout the simulation. The minimum value of $\eta k_{\max}$ at the end of the simulation is 1.2.

The boundary conditions for the dependent variables u_i, f, and p are periodic in the streamwise (x) and spanwise (y) directions. The boundary condition in the direction of the imposed mean velocity gradient (z) is shear-periodic in the case of homogeneous shear and periodic for the nonsheared flow. Stated mathematically, for the variable ϕ,

$$\begin{aligned} &\phi \in \{u_1, u_2, u_3, f, p\}, \\ &\phi(t, x_1 + m_1, x_2 + m_2, x_3 + m_3) \\ &\quad = \phi[t, x_1 - S(x_3 + m_3)t, x_2, x_3], \end{aligned} \tag{14}$$

where m_i are arbitrary integers (integer multiples of L). In order to justify the use of periodic boundary conditions in turbulence simulations, the integral length scales must remain sufficiently small relative to the computational domain L. In our simulations, the integral length scale does not exceed $0.15L$. A further check was made by evaluating the two-point velocity correlation

$$R_{11}(r_1) = \langle u_1(x_1) u_1(x_1 + r_1)\rangle / \sqrt{\langle u_1^2(x_1)\rangle}\sqrt{\langle u_1^2(x_1)\rangle},$$

which measures the enhanced spatial correlation in the streamwise direction due to shear. The simulations were terminated at a nondimensional time of $t=8$ beyond which $R_{11}(r_1)$ in the shear flows begins to attain nonzero values at the half-box width $r_1 = L/2$.

Complete details of the numerical solution procedure are given elsewhere.[17,20] It suffices here to state that the governing equations are discretized in an Eulerian framework using a second-order finite-difference method on a staggered grid for all the terms except those corresponding to the mean advection, where pseudospectral approximation is used. Integration in time is performed via the Adams–Bashforth scheme. Pressure is treated implicitly and obtained using a Poisson solver, which includes the shear-periodic boundary conditions. The 128^3 grid simulations were performed on a Cray Y-MP 8/864 and required approximately 32 megawords of core memory. Execution time for the shear flow computations is approximately 7.0 sec per time step. Typical runs involve 2048 time steps.

III. RESULTS

A. General flow characteristics

Results are presented for four flow conditions. Two homogeneous shear flows are considered, differing only in the initial value of the strain number, St_0. In one case, $\mathrm{St}_0 = 1.0$, referred to hereinafter as case H (high initial strain), and in the other, $\mathrm{St}_0 = 0.33$, referred to as case L (low initial strain). The other two flows are those of decaying grid turbulence (cases IH and IL) having the same initial large-scale strain rate (v_0/l_0) as cases H and L, respectively. A summary of initial- and final-run parameters is given in Table I. It should be noted throughout the results presented that the time t is dimensionless and equals the real time normalized by L/U.

TABLE I. Summary of flow parameters.

Time	Parameter	IH	IL	H	L
	Re_{λ_0}	25.0	25.0	25.0	25.0
	St_0 or v_0/ℓ_0	1.0	0.32	1.0	0.33
	ν/η_0^2	7.76	2.60	4.71	1.57
0.	ℓ_0	0.0515	0.0515	0.0469	0.0469
	λ_0	0.0236	0.0236	0.0380	0.0380
	η_0	0.0024	0.0024	0.0039	0.0039
	ν	0.000 047	0.000 016	0.000 071	0.000 024
	ηk_{max}	1.0	1.0	1.6	1.6
	Re_λ	17.5	18.7	28.5	37.5
	St or v/ℓ	0.10	0.09	0.34	0.34
	ν/η^2	0.91	0.85	2.24	2.49
8.	ℓ	0.1333	0.0876	0.1007	0.0716
	λ	0.0589	0.0363	0.0590	0.0367
	η	0.0072	0.0043	0.0056	0.0030
	ηk_{max}	2.9	1.7	2.3	1.2

Figure 3 shows the time development of the characteristic strain rates associated with the large scale (v/ℓ) and small scale (ν/η^2) for the four cases. The time development of the normalized integral and Kolmogorov length scales is shown in Fig. 4. As expected, the small-scale strain dominates over the large-scale strain although the difference in magnitudes is limited by the moderate value of Reynolds number used. The decrease in strain rates for grid turbulence (IH and IL) is evident. In the shear case H, the effects of turbulence initially dominate over those of the mean flow causing the strain rates to decrease until a time of $t = 6$ at which the small-scale strain begins to increase. The Kolmogorov scale correspondingly increases initially then decreases after $t = 6$ (Fig. 4). For the shear case L, a steady increase in the small-scale strain rate occurs because of the decreasing Kolmogorov length scale as shown in Fig. 4. Note that the time development of the large-scale strain (v/ℓ) in Fig. 3 for the shear cases is also that of the strain number St, since $S = 1$ in Eq. (11).

A measure of the smallest scales in the scalar field is the scalar microscale $L_C = (D^3/\epsilon)^{1/4}$, often referred to as the Obukhov–Corrsin scale. Since the molecular viscosity and diffusivity are constant in our flows (and $Sc = \nu/D = 0.7$), the development of L_C follows that of η. In an inhomogeneous scalar field, length scales associated with the scalar will exhibit spatial dependence. A scalar length scale reflecting this inhomogeneity is the dissipation scale λ_f defined by

$$\lambda_f = (6D\langle f'^2\rangle/\langle\epsilon_f\rangle)^{1/2}, \tag{15}$$

or in terms of its directional components,

$$\lambda_{fi} = \left(\frac{6\langle f'^2\rangle}{\langle(\partial f'/\partial x_i)^2\rangle}\right)^{1/2}, \quad i = 1,2,3. \tag{16}$$

The time development of the λ_f and λ_{fi} profiles in the x_3 or z direction was determined. In the isotropic flow, the component scales remain approximately equal within the mixing zone, i.e., $\lambda_{f1} = \lambda_{f2} = \lambda_{f3}$. In shear flow, the component scales exhibit differences, with the time rate of increase being largest for the streamwise component λ_{f1} and the smallest for the transverse (z) component λ_{f3}. This is due to the directional alignment of the rate of strain axes and their interaction with the scalar gradient, as will be discussed later. In both isotropic and shear cases, the time development of λ_f tends to follow that of λ, indicating the strong influence of the flow field.

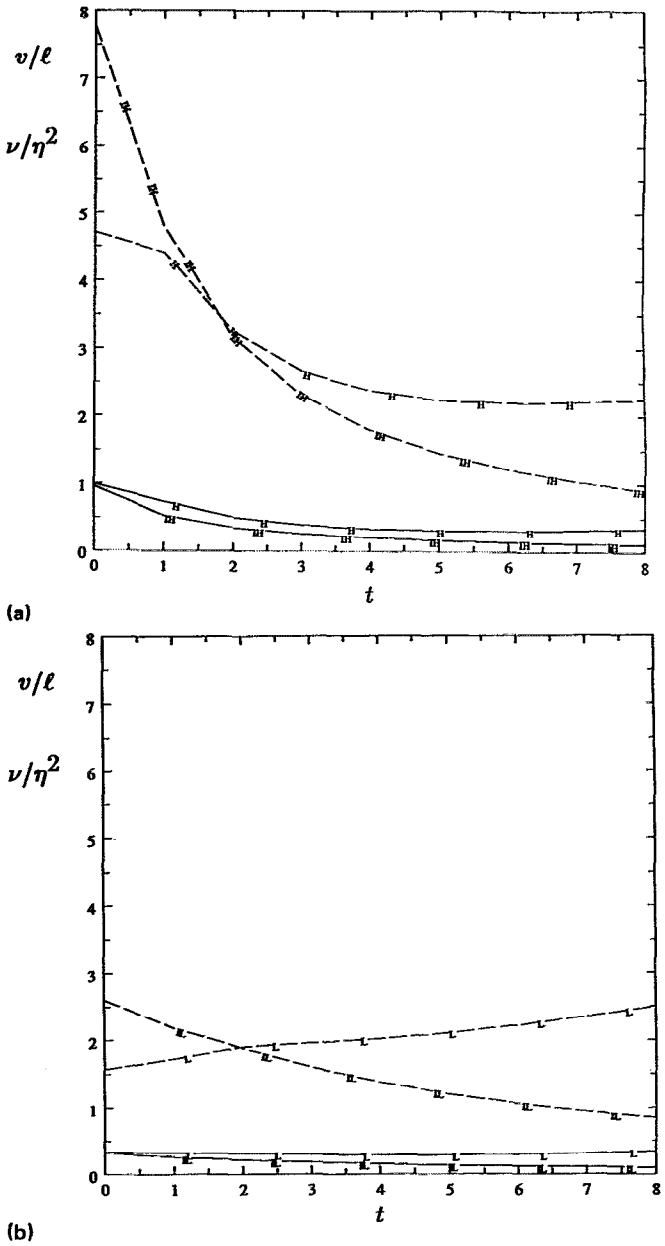

FIG. 3. Time development of characteristic strain rates, large-scale, v/ℓ(——) and small-scale, ν/η^2 (– – –). (a) Cases IH and H ($St_0 = 1.0$), (b) cases IL and L ($St_0 = 0.33$).

B. Strain rate and vorticity statistics

Turbulence generates the largest strain rates at the smallest scales. Thus the small-scale strain rate ν/η^2 is a measure of the dominating strain rates in turbulent flows. However, the variation of the components of the strain-rate tensor throughout the flow field affects the scalar mixing and

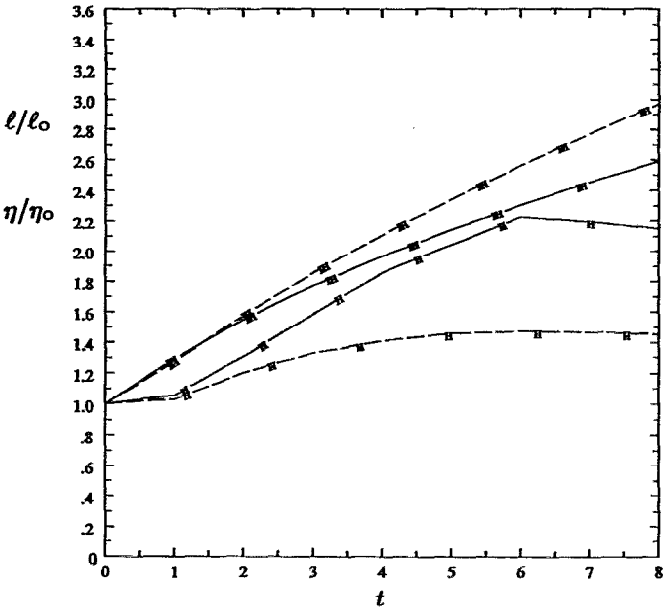

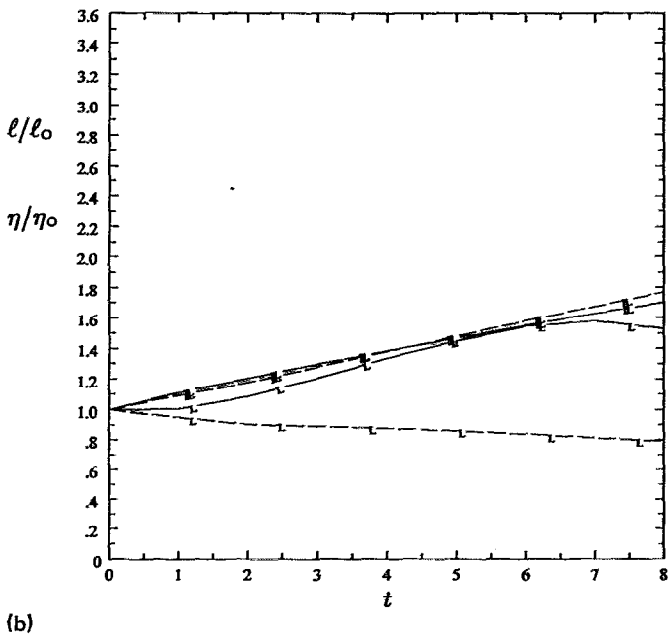

FIG. 4. Time development of normalized integral length scale, ℓ/ℓ_0 (——) and Kolmogorov length scale, η/η_0 (– – –). (a) Cases IH and H ($St_0 = 1.0$), (b) cases IL and L ($St_0 = 0.33$).

the dynamics of the reactive interface. The strain-rate tensor $e_{ij} = 1/2\{\partial u_i/\partial x_j + \partial u_j/\partial x_i\}$ at each computational grid point can be evaluated from the computed velocity field. Since it is the instantaneous values of e_{ij} that are of interest for the statistics, the mean velocity gradient is included in the shear flow cases. The eigenvalues and eigenvectors of the principal strain rates are determined following the general method described by Timoshenko and Goodier.[21] The eigenvalues are ordered by $\alpha \geqslant \beta \geqslant \gamma$, where α is always positive (most extensional), γ is always negative (most compressive), and β is either positive or negative (intermediate) depending on the magnitudes of α and γ. This follows from the continuity equation for incompressible flows, i.e., that the sum of these diagonal components is zero ($\alpha + \beta + \gamma = 0$).

Statistics of the flow field are obtained by sampling over the entire computational domain. The intermediate strain rate β is found to be extensional (positive) at approximately 75% of the points in both the isotropic and homogeneous shear flows, which is consistent with the results of Ashurst *et al.*[9] and Leonard and Hill.[13] This gives, on the average, two positive and one negative strain-rate eigenvalues. Betchov[22] showed that the product of the strain rate eigenvalues is related to the velocity derivative skewness in isotropic turbulence:

$$\langle \alpha\beta\gamma \rangle \sim S_1, \tag{17}$$

where

$$S_1 = \frac{\langle (\partial u_1/\partial x_1)^3 \rangle}{\langle (\partial u_1/\partial x_1)^2 \rangle^{3/2}}. \tag{18}$$

The velocity derivative skewness can be related to vorticity production and appears in the enstrophy transport equation derived for isotropic flow:[23]

$$\frac{\overline{d\omega_1^2}}{dt} = -\frac{7}{3\sqrt{5}} S_1 (\overline{\omega_1^2})^{3/2} - 10\nu \overline{\left(\frac{d\omega_1}{dx_1}\right)^2}. \tag{19}$$

The second term on the right side of (19) is always negative and represents the destruction of mean square vorticity by viscous dissipation. In order to maintain vorticity fluctuations and hence turbulence, there must be a production term. Thus the first term must be positive, hence $S_1 < 0$. As concluded by Betchov,[22] there must be a predominance of two positive principal strains in order to have vorticity production; the mechanism involved being vortex stretching. Figure 2 shows the total skewness remaining negative

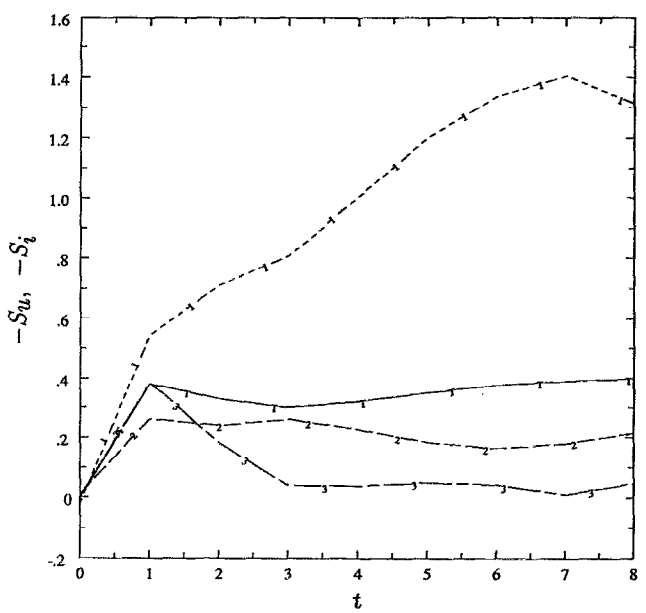

FIG. 5. Time development of the velocity derivative skewness components, $-S_i$ ($i = 1,2,3$), for shear case L in the directions of x_1 (- - - -), x_2 (– – –), x_3 (— · —), and the total value (——).

$(-S_u > 0)$ for all four cases. As mentioned, the skewness is a measure of spectral energy transfer. The expected increase of energy transfer in shear flow is evident from the time development of the streamwise component of the skewness S_1. Figure 5 shows the three directional components of the skewness for the shear case L. Note that the growth of $-S_1$ is accompanied by a reduction in the other two components. More generally, the equation for enstrophy transport is written as

$$\frac{D}{Dt}\left(\frac{1}{2}\omega_i^2\right) = \omega_i\omega_j e_{ij} + \nu\frac{\partial^2}{\partial x_j \partial x_j}\left(\frac{1}{2}\omega_i^2\right) - \nu\frac{\partial \omega_i}{\partial x_j}\frac{\partial \omega_i}{\partial x_j}, \tag{20}$$

where $\omega_i\omega_j e_{ij}$ is the general form of the vorticity production term, the components of which are shown in Fig. 6. It is seen that, in both the isotropic and homogeneous shear flows, the time development of $\omega_i\omega_j e_{ij}$ follows the general behavior of the product of the strain-rate eigenvalues $-\langle\alpha\beta\gamma\rangle$, which in turn, follows that of the small-scale strain ν/η^2 (Fig. 3).

Probability distributions of the principal rates of strain normalized by the total strain magnitude $|e| = (\alpha^2 + \beta^2 + \gamma^2)^{1/2}$ are given in Fig. 7. The number of bins used in the sampling is 40 giving a bin width of 0.05. Initially, at $t = 0$ [Fig. 7(a)], the distributions are symmetric and the peak for the intermediate strain probability occurs at $\beta = 0$. This is a consequence of the random initial velocity fields used in the simulations. The development to

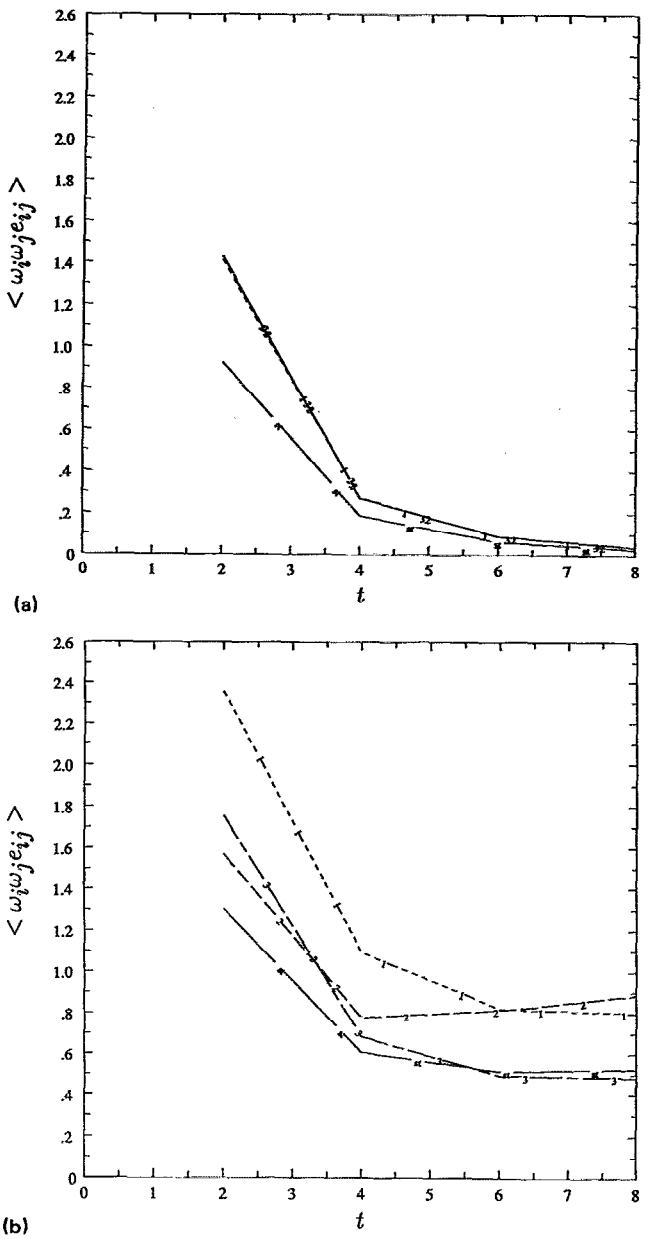

FIG. 6. Time development of vortex production term $\langle\omega_i\omega_j e_{ij}\rangle$ components: x_1 (----), x_2 (– – –), x_3 (— — —), and $-\langle\alpha\beta\gamma\rangle$ (—st—); for (a) case IH (isotropic) and (b) case H ($St_0 = 1.0$).

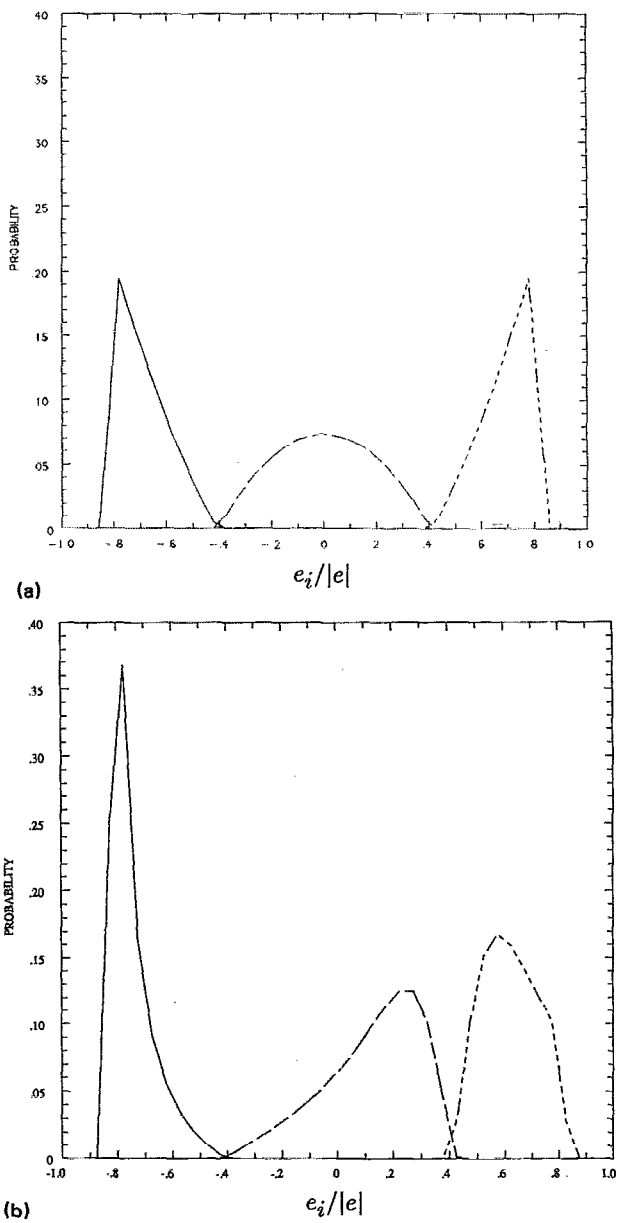

FIG. 7. Probability distributions of the principal strain rates (normalized by total strain magnitude) at (a) $t = 0$ and (b) $t = 6$, for case H ($St_0 = 1.0$); γ: (——), β: (– – –), α: (----).

an asymmetric form [Fig. 7(b)] occurs fairly rapidly, within the first time unit, which corresponds to one initial eddy turnover time ℓ_0/v_0 for cases H and IH and one-third initial eddy turnover for cases L and IL. Beyond this time, the profiles remain approximately invariant. The shape of the distributions is similar for all four flow conditions suggesting a universal strain structure.[9] The most probable value of the normalized β strain tends toward 0.2 causing the compressive strain pdf to steepen at a higher (negative) value, since the sum of the strain components must be zero. As indicated in the figures, the most probable ratio of the strain rates is $3{:}1{:}-4$ ($\alpha{:}\beta{:}\gamma$), which agrees with the results of Ashurst *et al.*[9] and Kerr.[24] The overall shape of the β distribution agrees closely with that given by Kerr, with a peak occurring at the same normalized value. Note that the slight overlap of the curves and the offset in peak values are due to the finite bin width and not from the data. The analyses of Ashurst *et al.* and Kerr were performed on stationary (forced) isotropic turbulence. We show here that similar results are obtained for decaying turbulence. This may be expected because of the self-preserving nature of the flow, where Re_λ remains constant.[25] The results of our isotropic turbulence simulations do exhibit a relatively constant Re_λ after the flow develops ($t > 2$).

The orientation of vorticity relative to the principal strain-rate directions is determined by evaluating the cosine of the angle between the vorticity vector and each of the strain-rate axes at each grid point in the domain. Figure 8 displays typical probability distributions of the direction cosines for the isotropic and shear flows. The distributions are generally similar in the two flows with an increased probability for the vorticity to align ($\cos\theta = 1$) with the intermediate β strain direction and normal ($\cos\theta = 0$) to the compressive γ strain direction. However, the probability for the alignment of vorticity and β is significantly higher in the shear case H than in the isotropic case IH. In both cases, alignment-conditioned values of vorticity are the highest when vorticity is aligned with the β strain. The expected value is approximately 1.5 to 2 times the value associated when the vorticity is orthogonal to β. Alignment-conditioned values of the vorticity production term $\omega_i\omega_j e_{ij}$ were also evaluated. We find early in the flow development ($t \leqslant 2$) in cases IH and H that higher vorticity production occurs when vorticity is aligned with the α and β strains rather than orthogonal to them. In the isotropic flow IH, the conditioned vortex stretching term is highest when vorticity is aligned with α, the magnitude being approximately 2.5 to 3 times the value associated with the orthogonal orientation. Throughout the development of the isotropic flow IH, the expected magnitude of $\omega_i\omega_j e_{ij}$ remains slightly higher when alignment is in the α rather than β direction. The same result is obtained when sampling is limited to those points where $\beta > 0$. This disagrees with Ashurst *et al.*,[9] who found that vorticity production is independent of the orientation with α. This may be due to the decreasing strain rates and vorticity fluctuations in our decaying isotropic flow. In sheared turbulence, vorticity production is highest when vorticity is aligned in the β direction. The alignment-conditioned values of $\omega_i\omega_j e_{ij}$ are two to seven times higher when vorticity is aligned with β rather than orthogonal to β; the relative difference increasing as the flow develops in time. The trend with respect to the α strain is opposite to that in the isotropic flow; higher production exists when vorticity is orthogonal to α.

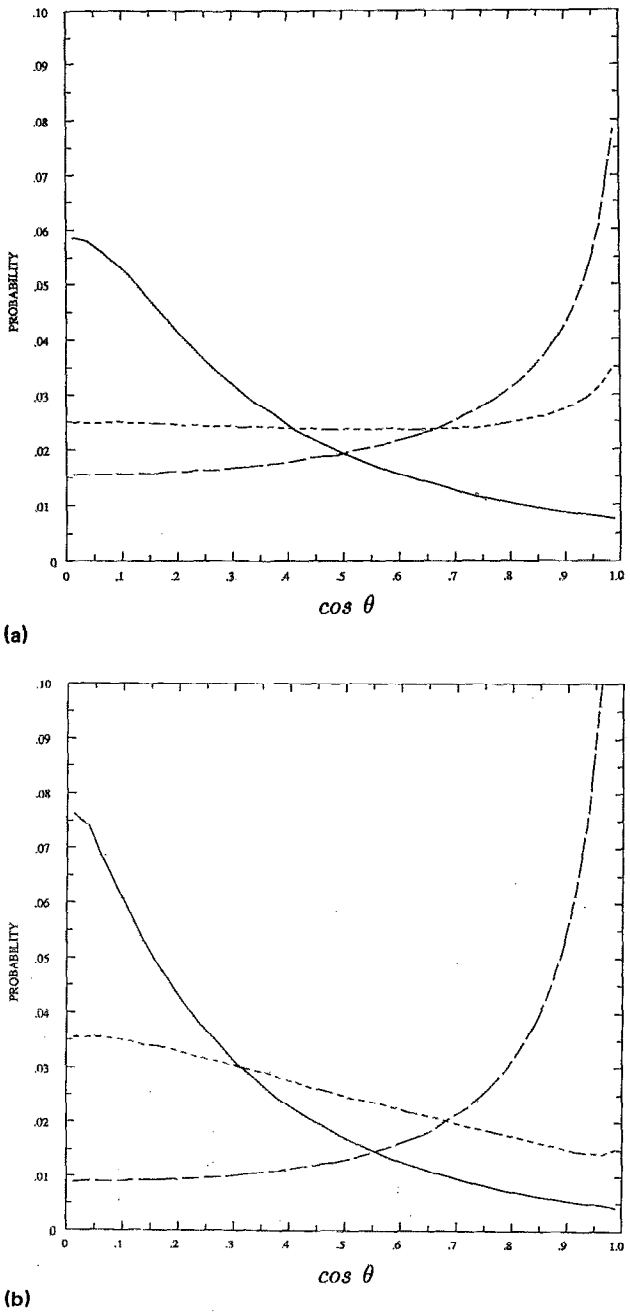

FIG. 8. Probability distributions of alignment of the vorticity vector and principal strain rate axes at time $t = 6$ for: (a) case IH (isotropic) and (b) case H ($\mathrm{St}_0 = 1.0$); γ: (——), β: (– – –), α: (- - - -).

As Betchov[22] showed, the process of vortex stretching, and therefore vorticity production, occurs when the intermediate strain rate is positive. DNS results presented here and those of Ashurst *et al.*[9] and Kerr[24] have further shown that the intermediate strain rate axis tends to align with the vorticity vector. Based on the conservation of angular momentum, we expect the vorticity to be amplified in the direc-

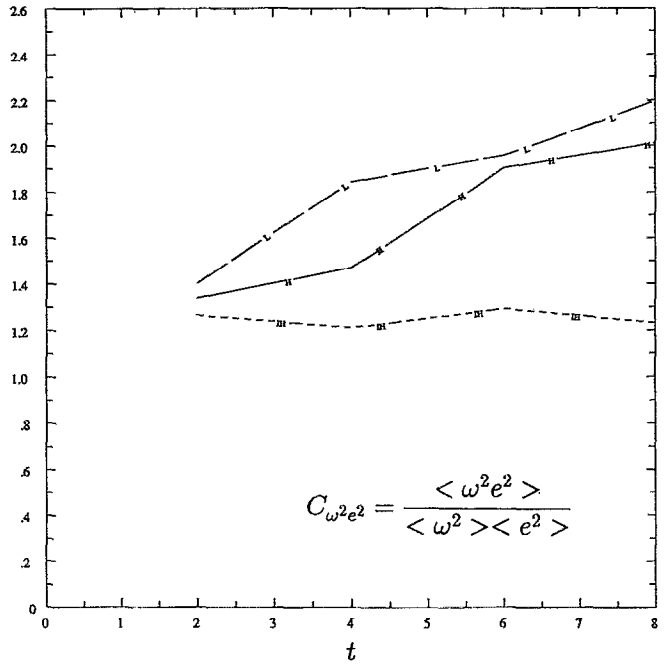

FIG. 9. Time development of vorticity-strain rate magnitude correlation coefficient $C_{\omega^2 e^2}$ for cases IH (- - - -), H (——), and L (– – –).

tion of positive strain and attenuated in the direction of negative strain. In the absence of viscosity, the product of vorticity and radius squared is conserved. Thus an increase in vorticity leads to a decrease in the scales of motion in the normal direction. The increase in the kinetic energy of rotation occurs at the expense of the velocity component in the direction of stretching, hence an increase in the velocity fluctuation components in the other two directions thus generating a new strain field. The sampled statistics indicate that the two strain components normal to the β strain tend to be significantly larger than β and comparable in magnitude to each other. Further evidence of the vorticity-induced strain field is given by the following correlation coefficient:

$$C_{\omega^2 e^2} = \langle \omega^2 e^2 \rangle / \langle \omega^2 \rangle \langle e^2 \rangle, \tag{21}$$

which correlates the magnitude of vorticity with that of the total strain rate and has an uncorrelated value of 1.0. The time development of $C_{\omega^2 e^2}$ is shown in Fig. 9. Note the higher values of $C_{\omega^2 e^2}$ in shear cases H and L, where significant production is occurring and the strength of the generated strain field increases in time. She *et al.*[11] have suggested that the probable alignment of ω with the β strain axes may be caused by the controlling influence of the vorticity on the strain field. This is further supported here by comparing the characteristics of decaying turbulence with those of shear-generated turbulence.

It has been argued that the predominance of two positive and one negative principal strain rates would lead to the formation of sheetlike structures in the flow.[22,24] She *et al.*[11] point out that the strain field typically varies over the lifetime and spatial extent of the structures, and therefore sheetlike formation will not necesarily take place. Furthermore, the structure itself modifies the surrounding strain field. Results of DNS have shown that the dominant structure for high-magnitude vorticity regions is tubelike.[8,9,11,12] Sheetlike structures also exist but at moderate values of vorticity.[11,12] High-magnitude tubelike structures exist in our decaying isotropic flow; however, they represent only a very small fraction of the entire volume. More prevalent are the moderate vorticity ($2\,\overline{|\omega|} < |\omega| < 3\,\overline{|\omega|}$) sheetlike structures and low-level "background" activity.[12] In sheared turbulence, the flow field is characterized by the presence of organized large-scale structures, as will be discussed below.

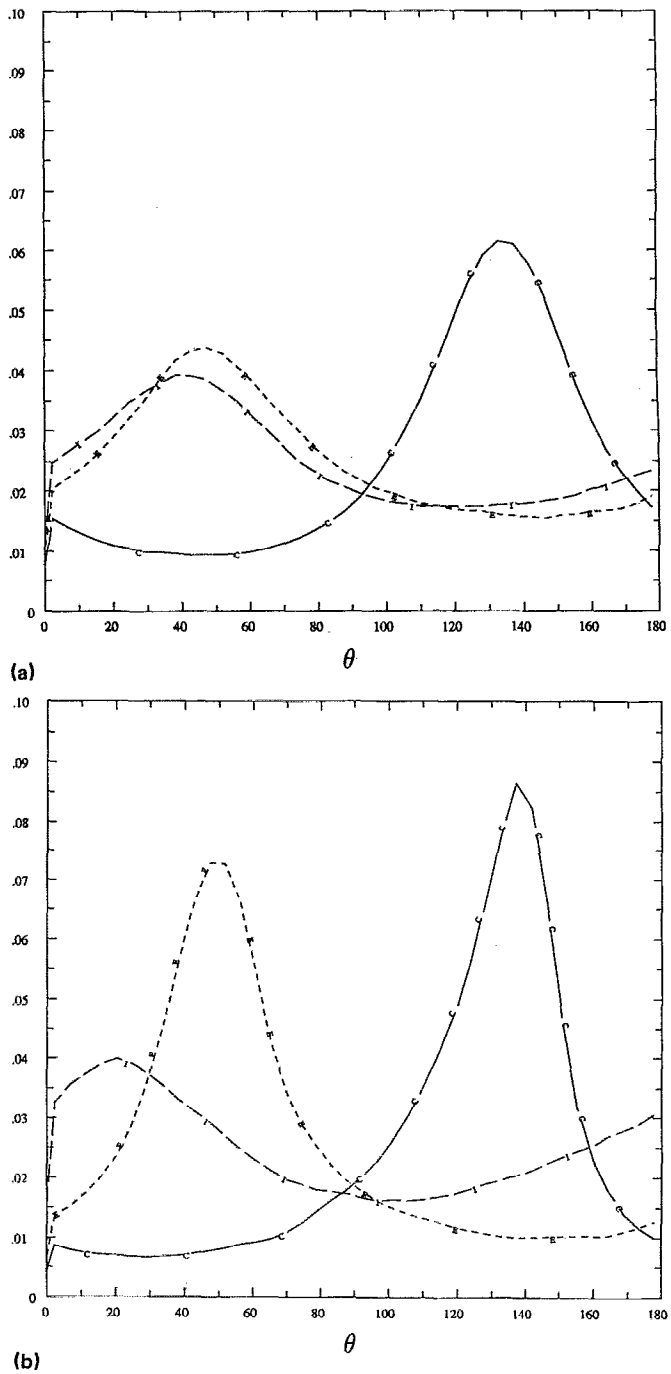

FIG. 10. Probability distributions of the inclination angle of the projected principal strain rate axes onto the x-z plane for case H at (a) $t = 2$, (b) $t = 8$; γ: (——), β: (– – –), α: (- - - -).

The orientation of the strain-rate axes in space is random for the isotropic cases, however, for the shear cases, a directional preference exists because of the presence of the mean strain component. This is examined by projecting the strain-rate axes onto the x-y (horizontal) and the x-z (vertical) planes (see Fig. 1 for coordinate axes). Figure 10 shows probabilities of the inclination angle of the projected principal strain axes onto the x-z plane for case H. Similar results are obtained for case L. The inclination angle is measured from the positive x axis. Initially (not shown), the strain field is basically two dimensional and follows the mean strain field; thus the α and γ strain components most probably align at 45° and 135° from the positive x axis, respectively. The β strain is small in magnitude and the inclination profile is relatively flat, i.e., no preferred direction. After the flow develops (beyond the initial growth of the velocity derivative skewness), the peaks in the inclination of the strain rates in the x-z plane become more pronounced and, in addition, a directional preference develops for the β strain [Fig. 10(a)]. The peak in the inclination angle profile of the β strain occurs first near the region of the most extensional strain peak. As the flow develops, the peak shifts toward smaller angles [Fig. 10(b)]. At $t = 8$, the peak in the β strain occurs at approximately 20°. The locations of the α and γ strain peaks remain fairly invariant in time because of the presence of the mean strain.

As expected, the vorticity field also exhibits distinct directional features in the presence of mean shear. The orientation of the vorticity vector in space is examined by projecting it onto the x-y (horizontal) and the x-z (vertical) planes. Figures 11 and 12 show the time development of the probability distribution of the inclination angle of the projected vorticity vector onto the x-y and x-z planes, respectively, for case H. In the x-y plane, the inclination angle is measured from the positive y axis, and, in the x-z plane, the angle is measured from the positive x axis. Initially, the spanwise component of vorticity (w_y) of the mean flow dominates as expected (indicated by a peak in probability at 0° in the x-y projection profiles; Fig. 11). The peak is more pronounced in case L (not shown), where the effect of mean strain is relatively higher. In time, the distribution develops "shoulders" around $\theta = \pm 90°$ indicating a modification of direction for a portion of the vorticity toward the x-z plane. The weighted distribution [Fig. 11(b)] shows that the relative magnitude of the vorticity near $\theta = \pm 90°$ (x-z plane) increases and becomes comparable to that at $\theta = 0°$ (y-z

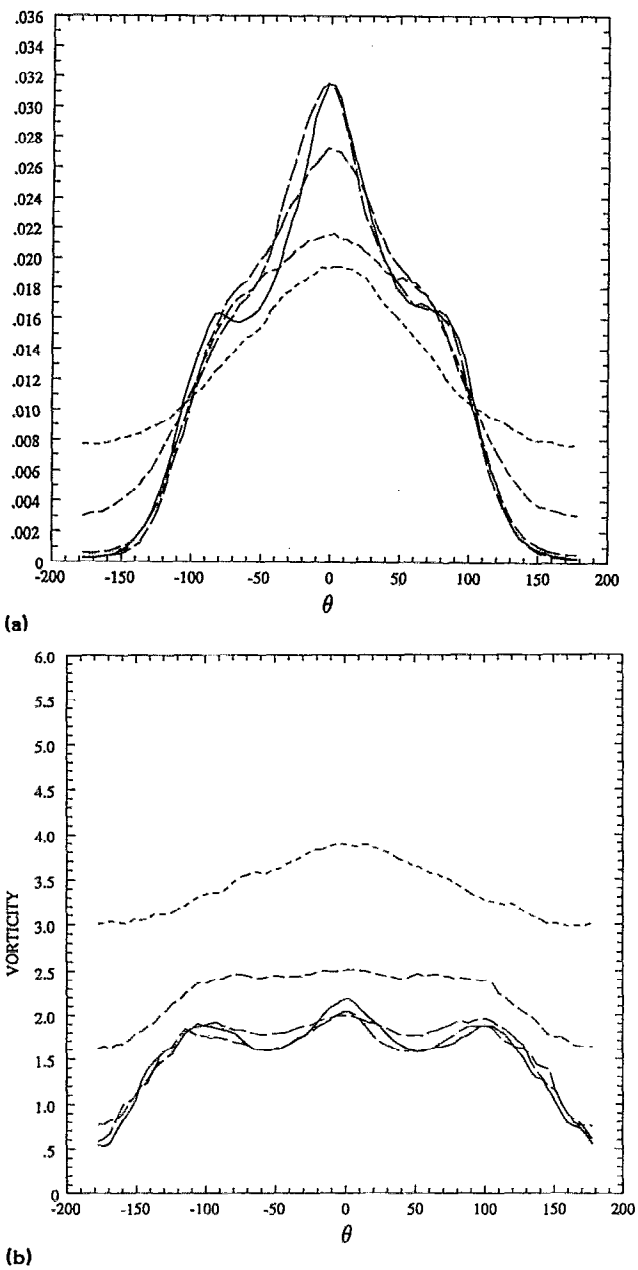

FIG. 11. Probability distributions of the inclination angle of projected vorticity vectors onto the x-y plane (θ measured from positive y axis) for case H ($St_0 = 1.0$): (a) (unweighted), (b) (weighted), at $t = 0$ (- - - -), $t = 2$ (– – –), $t = 4$ (——), $t = 6$ (— - —), and $t = 8$ (——).

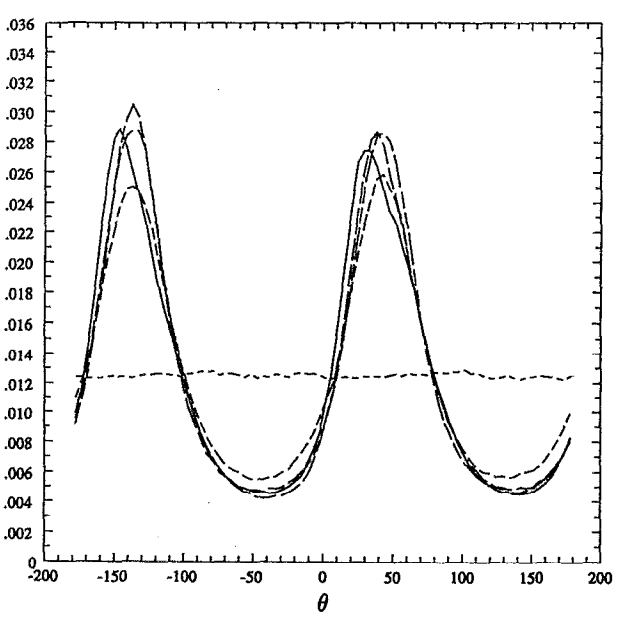

FIG. 12. Probability distributions of the inclination angle of projected vorticity vectors onto the x-z plane (θ measured from positive x-axis) for case H ($St_0 = 1.0$) at $t = 0$ (----), $t = 2$ (– – –), $t = 4$ (——), $t = 6$ (— - —), and $t = 8$ (——).

plane). Probability distributions in the x-z plane (Fig. 12) show that, initially, there is no directional preference due to the isotropic initial condition. As the flow develops, a preferred inclination appears near an angle of 45° (or $-135°$) from the positive x axis, in agreement with Rogers and Moin[10] and Moin and Kim.[26] The magnitude-weighted distribution (not shown) exhibits a similar profile indicating that vorticity is augmented when oriented in that direction. Further development causes the predominant angle of inclination to decrease, i.e., move toward the x axis. At time $t = 8$, this angle is approximately 30° for both cases H and L. This generally follows the unweighted inclination angle distribution of the β strain (Fig. 10), as expected because of the high probability of alignment between the vorticity and intermediate strain. The shift toward smaller angles is caused by the rotation component of the applied shear.

The vorticity field of a flow with mean shear is characterized by the presence of organized large-scale structures. Hairpin-shaped vortex structures in an inclined plane at $\theta \leqslant 45°$ (from the x axis), similar to those found by Rogers and Moin,[10] are observed in our shear flow simulations. These structures are formed because of the deformation of transverse vorticity (w_y) by the mean strain.[26] Sheetlike regions of moderate to high values of vorticity ($2\,\overline{|\omega|} < |\omega| < 3\,\overline{|\omega|}$) also exist and occur in the inclined planes. Further discussion of these structures will be given in the next section.

In general, our analysis of the strain rate and vorticity characteristics supports the conclusions given by Ashurst *et al.*[9] and Kerr.[8,24] Turbulent flows consist of stretching vortex structures. These structures are tubelike at high values of vorticity and sheetlike at moderate vorticity.[11,12] Vorticity is amplified by axial stretching along the intermediate strain direction, thus generating larger strains in the plane perpendicular to the elongated vortex structures. The distinct directional preference of the strain rate and vorticity fields and their associated structure in homogeneous sheared turbulence have significant effects on the characteristics of the scalar mixing field as discussed below.

C. Scalar mixing characteristics

Since chemical reaction in our flow is assumed to occur instantaneously, the reaction is controlled by turbulent mixing. The flame sheet is represented by the stoichiometric isoscalar surface. The normal vector to this surface coincides with the local scalar-gradient vector ∇F. Orientation of an isoscalar surface with respect to the principal strain axes is determined from the direction cosines between the scalar gradient and the strain-rate axes. Alignment probability distributions are obtained by sampling the *mixed* scalar field, which we have arbitrarily defined as those points with a mixture fraction value in the range $0.1 \leqslant F \leqslant 0.9$. The initial homogeneous unmixed scalar regions are thereby eliminated from the statistics. Results are given in Fig. 13 for $t = 6$. For the isotropic flow [Fig. 13(a)], there is an increased probability for ∇F to align in the direction of the most compressive γ strain and to align perpendicular to the extensional α and β strains. Isoscalar (or isoconcentration) surfaces thus tend to be stretched in isotropic flows. The compressive strain brings these surfaces closer together amplifying the scalar-gradient fluctuations. This results in the generation of scalar fluctuation at the high wave-number end of the spectrum. The effect of molecular diffusion is to smear out the fluctuation gradients. Since the rate of diffusion is directly proportional to the scalar gradient, high wave-number components are favored in this process. This is the general mechanism for the production of fine structure in scalar fields in isotropic turbulence.

In shear flow [Fig. 13(b)], alignment between ∇F and the α and γ strains differs from that of the isotropic flow case although the alignment between the scalar gradient and β strain is similar and tends to occur at 90° ($\cos\theta = 0$). Align-

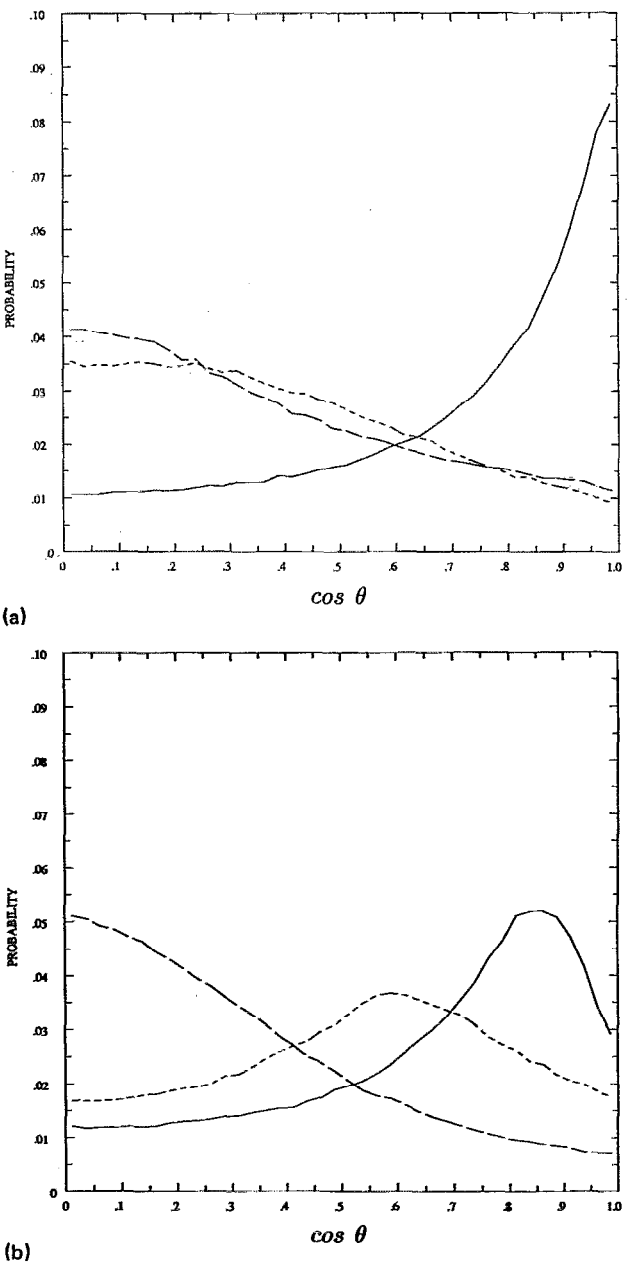

FIG. 13. Probability distributions of alignment of the scalar gradient vector and principal strain rate axes at time $t = 6$ for (a) case IH (isotropic) and (b) case H ($St_0 = 1.0$). γ: (——), β: (– – –), α: (- - - -).

ment of the scalar gradient and γ strain tends to occur at $\theta \simeq 30°$ ($\cos\theta = 0.86$). Alignment with the α strain direction occurs at approximately $\theta \simeq 55°$ ($\cos\theta = 0.58$). Similar results were reported by Ashurst *et al.*[9] and Leonard and Hill[16] although explanations for the observations were not given. The skewed alignment of the scalar gradient with both the most compressive and most extensional strains in the shear flows is a result of the interaction of the imposed mean scalar gradient and mean strain rates with the turbulent fluctuations. Examination of the time development of the compressive and extensional strain alignment probability distributions for case H (Fig. 14) clarifies this. At early time ($t = 2$), the scalar gradient tends to align with the compressive strain [Fig. 14(a)] and, correspondingly, aligns normal to the extensional strain [Fig. 14(b)], and is therefore similar in behavior to isotropic turbulence. This is due to the high turbulent strain rates existing initially in the flow, which are much greater than the mean strain ($\mathrm{St}_0 = 1$ and $\nu/\eta^2 = 4.7$). If the mean gradients of the velocity and scalar were dominating, the alignment peak would be expected to occur at 45° ($\cos\theta = 0.7$) for both curves. Later in time, the peaks do tend to shift toward $\cos\theta = 0.7$. Case L at early times (not shown) already shows the shifts due to the greater effect of the mean strains. There is a competing effect between the turbulence and mean gradients and as the flow field develops, the effects of the mean flow appear to dominate, thus causing the alignment probability peaks to shift away from those of isotropic turbulence. Strain alignment characteristics of a passive scalar will therefore depend on the orientation of imposed mean gradients and the relative magnitude of the turbulent strain to mean strain.

A visual display of the strain rate–scalar gradient interaction is provided in Fig. 15, which shows contours of instantaneous isoscalars superimposed on vectors indicating the inclination of the axis of the local most compressive strain γ in the center x-z (vertical) plane for cases IH and H. Note the predominance of a preferred direction for the γ strain in the shear flow case (135° or $-45°$ from the positive x axis, disregarding arrowheads) and the resulting directionality of the isoscalar contours; in contrast with the random orientation of the isotropic strain field of case IH. The isoscalar contours in both cases are plotted using the same contour interval. In case H, we see that the contours are much closer together than in case IH, indicating a locally higher scalar gradient due to the higher magnitudes of γ.

Since the isoscalar surfaces tend to align parallel to the β strain, it is expected that these surfaces will also lie parallel to the local vorticity vectors. Alignment statistics of ∇F and ω (not shown) confirm that the most probable relative orientation is orthogonal. Figure 16 shows contours of the instantaneous spanwise vorticity ω_y in a vertical (x-z) plane for cases IH and H (same plane as Fig. 15). Superimposed on these contours is the stoichiometric isoscalar surface of $F = F_{st}$. It is seen that the reactive interface (thickened for clarity) follows the vortex structures in both flows. In general, the observed isoscalar contours in the x-z plane [Figs. 15(b) and 16(b)] are more ordered in the shear flow because of the directional preference of the vorticity and strain-rate axes. Contours of streamwise vorticity in the y-z plane

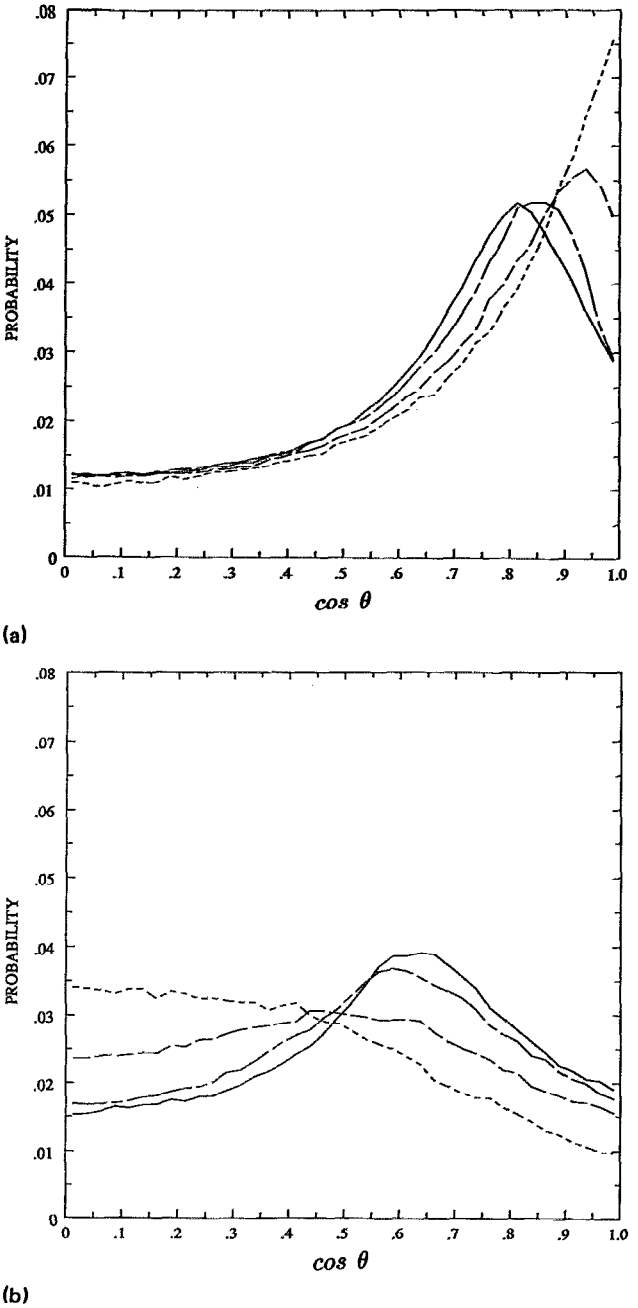

FIG. 14. Time development of the probability distributions of alignment of the scalar gradient vector and principal strain rate axes. (a) Case H: γ strain and (b) case H: α strain; $t = 2$ (– – –), $t = 4$ (— —), $t = 6$ (— · —), and $t = 8$ (——).

for the shear flow (not shown) are similar in nature to those in the x-z plane for isotropic flow [Fig. 16(a)]. Examination of a series of these cross-sectional views at later times indicate the existence of tubelike vortex structures. At time $t = 6$, the streamwise extent of some of these structures is roughly $L/4$ to $L/3$ long. The isoscalar surfaces are seen to wrap around these tubes and, in some cases, the scalar surface closes on itself and subsequently breaks away. The surfaces appear to be rotated by the local vorticity or stretched between two counter-rotating regions.

It has been suggested[27] that the small-scale scalar field

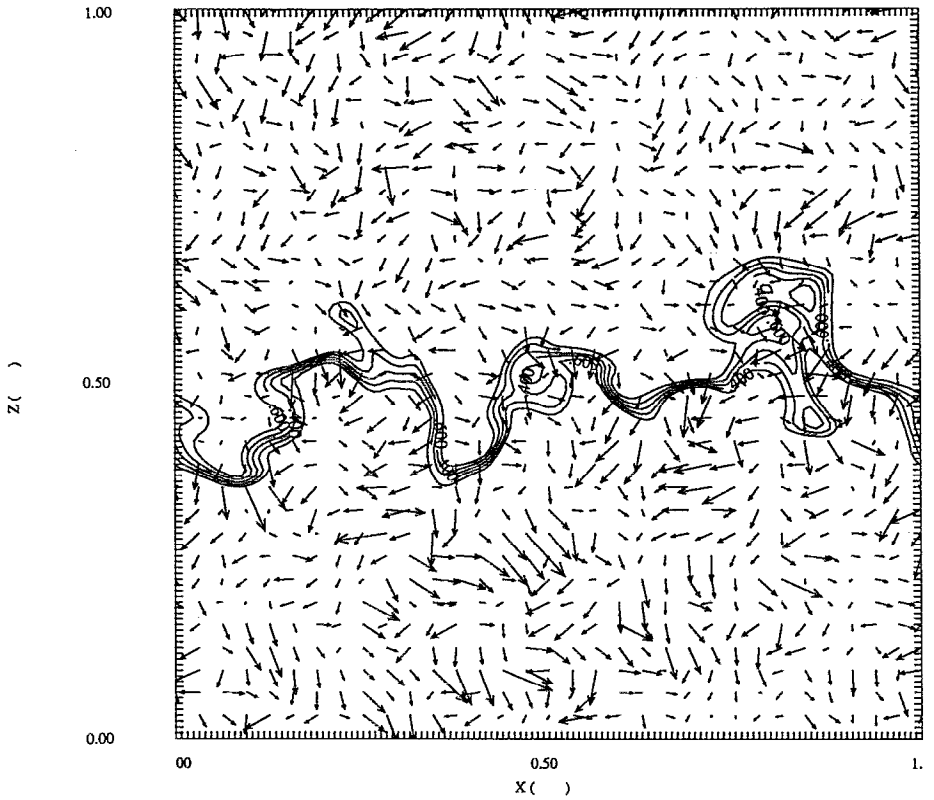

(a)

FIG. 15. Instantaneous most compressive (γ) strain rate axes projected on a vertical (x-z) plane with isoscalar contours ($0.3 < F < 0.7$) at time $t = 6$. (a) Case IH (isotropic) and (b) case H ($St_0 = 1.0$).

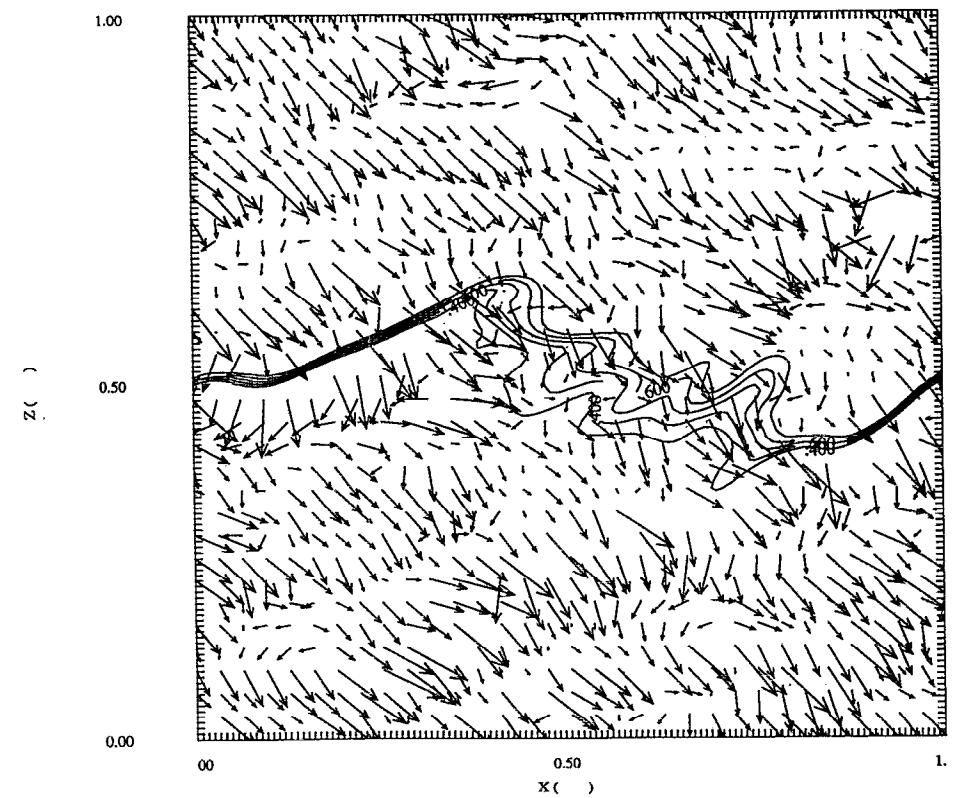

(b)

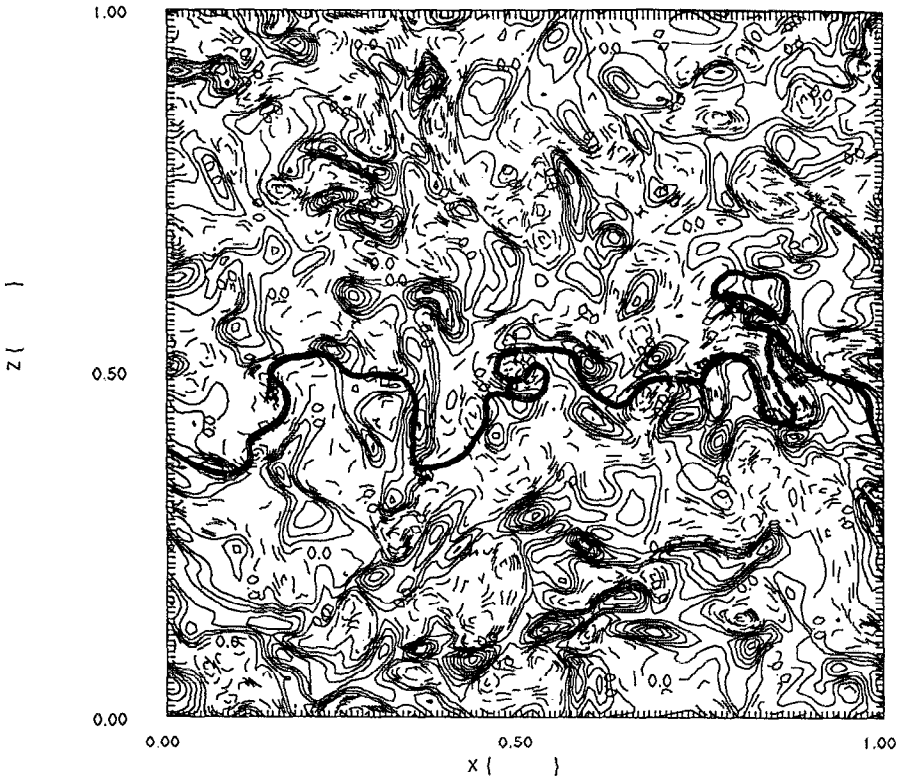

(a)

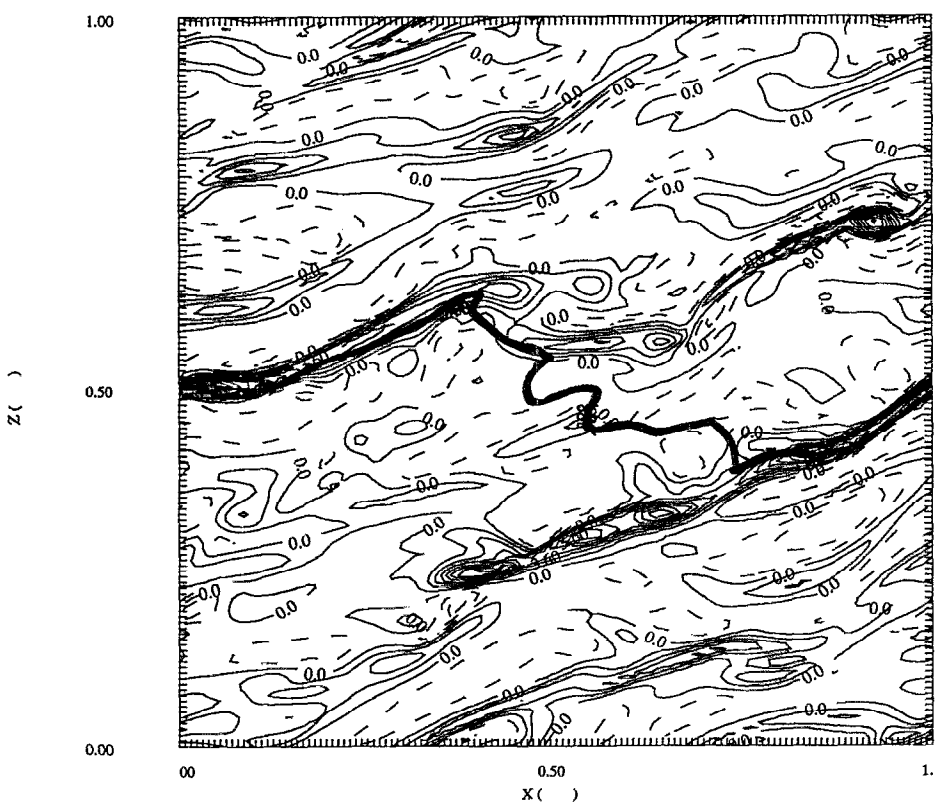

(b)

FIG. 16. Instantaneous contours of vorticity w_y projected on a vertical (x-z) plane with isoscalar contour line $F = F_{st}$ at time $t = 6$ for (a) case IH (isotropic) and (b) case H ($St_0 = 1.0$). Solid lines indicate positive vorticity, and dashed lines indicate negative vorticity.

may tend to develop sheetlike structures because of the influence of the long-lived large-scale motion, particularly in the case of flows with mean shear. Three-dimensional isoscalar surfaces of a high scalar-gradient magnitude (approximately ten times the total volume average) are shown in Fig. 17. We see that regions of high $|\nabla F|$ tend to be sheetlike in both isotropic and shear flow. In the former case, the structures are more intermittent while, in the latter, the sheets are continuous over a greater spatial extent. A close-up of a representative structure in each case is given in Fig. 18. Vortex lines in the vicinity of the structures are also displayed. In both cases, the vortex lines indicate a sheetlike structure that correspondingly forms a sheetlike structure for high scalar-gradient magnitudes. Note that the primary structure and associated vortex lines shown for the shear case [Fig. 18(b)] correspond to the inclined high-gradient region appearing on the left-hand side of Fig. 15(b) and the corresponding inclined high-vorticity region in Fig. 16(b). The sheetlike vortex structure in Fig. 18(b) is composed mainly of spanwise vorticity, which extends out for a distance of roughly $L/6$ or 1.5ℓ in the spanwise direction and $L/3$ in the streamwise direction. The local magnitude of vorticity prevailing throughout most of this region is in the range $2\ \overline{|\omega|} < |\omega| < 3\ \overline{|\omega|}$. As shown by Fig. 15(b), the compressive strain field associated with the structure acts in the orthogonal direction. The sheetlike nature of the vortex structure appears to provide a relatively unidirectional strain field

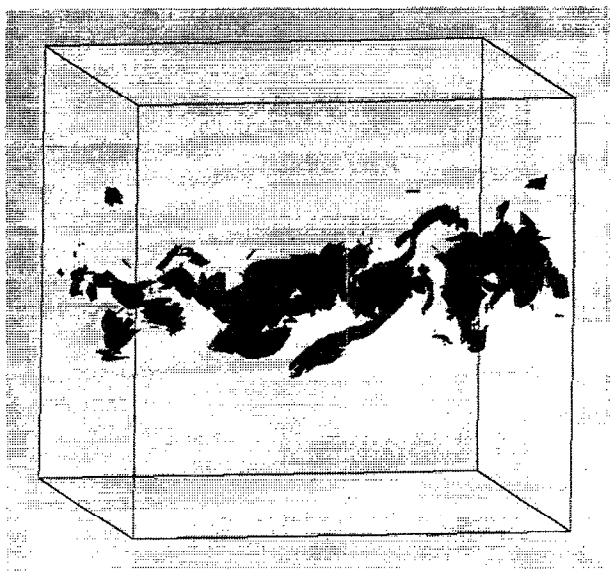

(a)

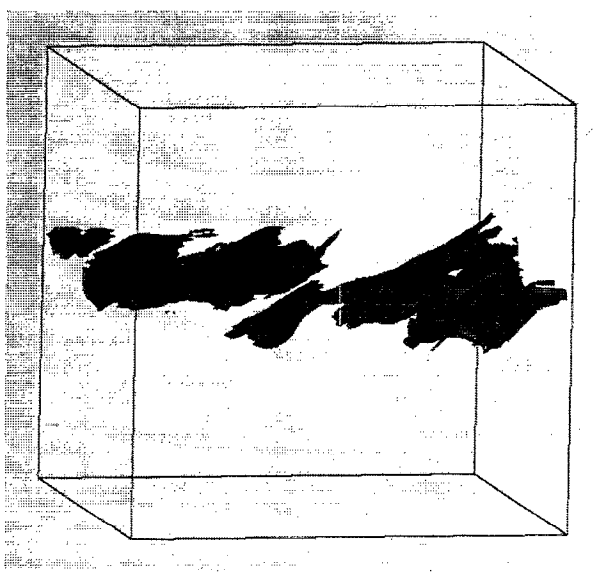

(b)

FIG. 17. Instantaneous isoscalar surfaces of a high scalar-gradient magnitude ($|\nabla F| \approx 10\ \overline{|\nabla F|}$) at time $t = 6$ for (a) case IH (isotropic) and (b) case H ($St_0 = 1.0$).

(a)

(b)

FIG. 18. Close-up views of instantaneous isoscalar surfaces of high scalar-gradient magnitude ($|\nabla F|$) along with neighboring vortex lines at time $t = 6$ for (a) case IH (isotropic): $|\nabla F| \approx 15\ \overline{|\nabla F|}$, and (b) case H ($St_0 = 1.0$): $|\nabla F| \approx 10\ \overline{|\nabla F|}$.

that effectively produces sheetlike structures in the $|\nabla F|$ field.

The correlation between the magnitudes of the strain rate and scalar gradient and between the vorticity and scalar gradient can be measured by the following correlation coefficients:[8]

$$C_{(\nabla F)^2 e^2} = \langle (\nabla F)^2 e^2 \rangle / \langle (\nabla F)^2 \rangle \langle e^2 \rangle,$$
$$C_{(\nabla F)^2 \omega^2} = \langle (\nabla F)^2 \omega^2 \rangle / \langle (\nabla F)^2 \rangle \langle \omega^2 \rangle, \quad (22)$$

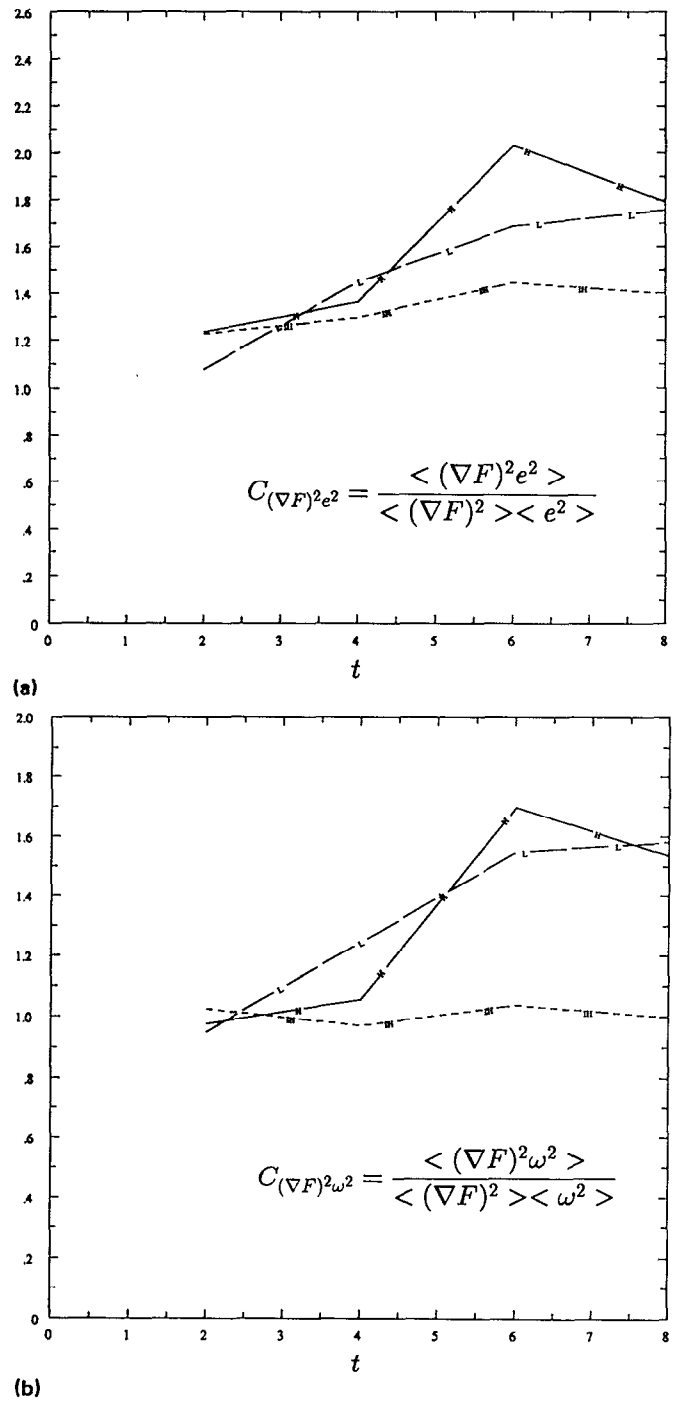

FIG. 19. Time development of scalar gradient-strain rate magnitude and scalar gradient-vorticity magnitude correlation coefficients. (a) $C_{(\nabla F)^2 e^2}$ and (b) $C_{(\nabla F)^2 \omega^2}$; for cases IH (- - - -), H (——), and L (– – –).

which are defined such that their uncorrelated value is 1.0. The time development of $C_{(\nabla F)^2 e^2}$ and $C_{(\nabla F)^2 \omega^2}$ is shown in Fig. 19. As expected, the magnitude of ∇F is clearly correlated with the strain rate in both flows, as shown by $C_{(\nabla F)^2 e^2}$ [Fig. 19(a)]. In Fig. 19(b), $C_{(\nabla F)^2 \omega^2}$ remains at the uncorrelated value of unity for the isotropic flow, which agrees with the results of Kerr[8] for stationary isotropic flow. However, in the shear cases H and L, values of $C_{(\nabla F)^2 \omega^2}$ greater than unity are exhibited, indicating that the magnitude of ∇F is correlated with that of vorticity in these flows.

Mechanisms influencing the scalar gradient are indicated by the scalar-gradient transport equation, which is obtained by taking the gradient of the scalar-transport equation

$$\frac{\partial \nabla F}{\partial t} + u \cdot \nabla (\nabla F) = -e \cdot \nabla F + \omega \times \frac{\nabla F}{2} + D \nabla^2 (\nabla F). \quad (23)$$

The first term on the right-hand side represents production of scalar gradient due to compressive strain alignment. Note that, as ∇F increases, further amplification increases indicating a positive feedback mechanism as described in Gibson's second mixing mechanism.[7] The second term, a cross product between the vorticity and scalar-gradient vectors, is a vector orthogonal to both ∇F and ω and, consequently, changes the direction of ∇F. This term is eliminated in the derivation of the transport equation for the square of the scalar gradient (proportional to the scalar dissipation rate), which is given by

$$\frac{D}{Dt}\left(\frac{1}{2} F_{,i}^2\right) = -F_{,i} F_{,j} e_{ij} + D \frac{\partial^2}{\partial x_j \, \partial x_j}\left(\frac{1}{2} F_{,i}^2\right) - D \frac{\partial F_{,i}}{\partial x_j} \frac{\partial F_{,i}}{\partial x_j}, \quad (24)$$

where $F_{,i} = \partial F / \partial x_i$. The fact that ω does not explicitly appear in the equation does not, however, imply that vorticity has no influence on the magnitude of ∇F. The contribution of ω can exist via its influence on the strain rate e (as indicated by $C_{\omega^2 e^2}$ in Fig. 9). This becomes apparent in sheared turbulence, where strain rates are amplified by vortex stretching as discussed earlier.

The overall form of Eq. (24) is similar to that of Eq. (20) for the transport of enstrophy, as noted by Corrsin.[28] The corresponding production term in the $(\nabla F)^2$ equation is $-F_{,i} F_{,j} e_{ij}$. This term represents gradient amplification by compressive straining (note the difference in sign of this term from that of enstrophy production) and thus reflects the influence of the strain rate on the scalar dissipation rate. A related quantity that various investigators have reported is the strain rate–scalar dissipation rate correlation coefficient given by

$$\Sigma = \langle \nabla F \cdot e \cdot \nabla F \rangle / \langle e : e \rangle^{1/2} \langle \nabla F \cdot \nabla F \rangle, \quad (25)$$

where e is the strain-rate tensor. Direct simulation results of Kerr[8] for forced isotropic turbulence give a value for Σ of -0.5. Leonard and Hill[16] report values in the range -0.5 to -0.4 for their isotropic runs.

Since our scalar field is inhomogeneous, we first determine the value of Σ conditioned on the value of the scalar F. The results indicate that Σ is independent of F. A representa-

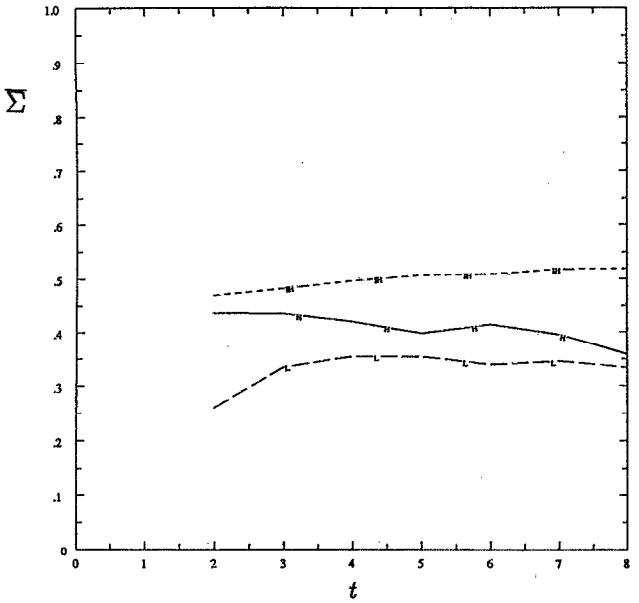

FIG. 20. Time development of strain rate–scalar dissipation correlation coefficient $\overline{\Sigma}$ for cases IH (- - - -), H (——), and L (– – –).

tive value of Σ can therefore be obtained by averaging over the range of F values $0.1 \leqslant F \leqslant 0.9$. Time development of the averaged $\overline{\Sigma}$ for cases IH, H, and L is given in Fig. 20. The value of $\overline{\Sigma}$ for the isotropic flow is about -0.5 and remains relatively constant in time. In shear flows, the magnitude of $\overline{\Sigma}$ is slighlty less and values range from -0.3 to -0.4. The negative value of Σ reflects the enhancement of the scalar gradient in the direction of the compressive strain. Based on the above results, the value of the correlation coefficient does not appear to be sensitive to the characteristics of the scalar field and is only slightly indicative of the presence of mean shear in the flow field.

D. Scalar dissipation rate

Chemical reaction is a molecular process and can only occur when mixing is complete at the molecular level. As stated earlier, the rate of molecular mixing, which is limited by the rate of breakup of "scalar eddies" containing the reactive species, is proportional to the rate of scalar dissipation. The rate of scalar dissipation, though it is a high-wave-number process, is determined by the interaction of the low-wave-number components of the velocity and scalar fields and is proportional to the mean rate of transfer of scalar variance from the low to high wave numbers. Regions of intense reaction have been found to correspond with local maxima of the scalar dissipation.[13,29]

The instantaneous scalar dissipation rate ϵ_F is defined as

$$\epsilon_F = D\left(\frac{\partial F}{\partial x_j}\right)^2 = \frac{\nu}{\mathrm{Sc}}(\nabla F)^2. \tag{26}$$

The distribution of the local instantaneous ϵ_F in the center x-z plane is shown in Fig. 21 (same plane as Figs. 15 and 16). Here, ϵ_F is graphically represented as vectors with magnitudes proportional to $(\nabla F)^2$ and in the direction of ∇F. Direct simulations of stationary isotropic turbulence by Kerr,[8] in which both the velocity and scalar fields are forced, have shown that scalar dissipation exists in intermittent patches with high magnitude. For our two-stream mixing flow, the locations of high scalar dissipation are confined to a narrow zone around the interface near $F = 0.5$. Within this zone, regions of peak ϵ_F do exist in sheets, as indicated by the structure of $|\nabla F|$. The intermittency of these sheets is less in sheared flow than in the unsheared flow because of the presence of the strong large-scale structures. This is of particular importance in reactive flows since, as stated above, intense reaction will occur in regions of high $(\nabla F)^2$, and therefore will occur in sheets.

From Fig. 21, we see that, in the isotropic flow (a), the magnitudes of ϵ_F are not significantly different from those in the shear case (b), even though the turbulence decays in the former with the associated increase in all length scales. This is explained as follows. Since ϵ_F is an instantaneous quantity, it depends on the mean scalar gradient and its fluctuations. The initially imposed scalar step function causes steep gradients of the mean scalar. The lower mixing rates in the isotropic flow allow significant scalar variance and mean gradients (∇F) to persist. In addition, the contribution of the small-scale motion to ϵ_F is limited because of the continuous growth of these scales, and therefore the corresponding fluctuating component of ∇F is small. In shear flows, the production of turbulent energy and increasing strain rates of the small scales augment the fluctuating component of ϵ_F. Local instantaneous scalar gradients can be quite large because of the increasing compressive strains. An indicator of the extent of scalar mixing is the probability density function (pdf) of the mixture fraction. Computed pdf's for a thin horizontal slab centered in the mixing zone indicate that the sheared cases exhibit the greatest extent of mixing. These profiles tend toward a Gaussian in time whereas those of the isotropic case retain a portion of the initial delta function peaks, indicating the presence of unmixed fluid.

It is of interest, from both physical and modeling standpoints, to examine the statistical distribution of ϵ_f. Gurvich and Yaglom[30] proposed a lognormal distribution of the scalar dissipation through an extension of Kolmogorov's third hypothesis. Experimental observations[31,32] suggest a lognormal distribution. The numerical simulations of Ashurst *et al.* show a lognormal distribution of the scalar dissipation rate,[29] and statistical independence of the scalar and scalar dissipation. Eswaran and Pope[33] have also performed direct simulations of forced isotropic turbulence with passive scalar "blobs." They showed that the probability density function (pdf) of the logarithm of scalar dissipation reaches an approximately Gaussian self-similar state. However, at the early stages of mixing, they find a strongly changing interdependence between the two variables.

The time development of the pdf of $\ln(\epsilon_F)$ for cases H and IH is shown in Fig. 22. The pdf's were obtained by sampling over the mixed fluid volume defined by $0.1 \leqslant F \leqslant 0.9$. The results show that the pdf of $\ln(\epsilon_F)$ approaches a nearly normal distribution with slight negative skewness. For the shear flow case H at later times, the skewness and kurtosis of the distributions are approximately -0.1 and 2.9, as com-

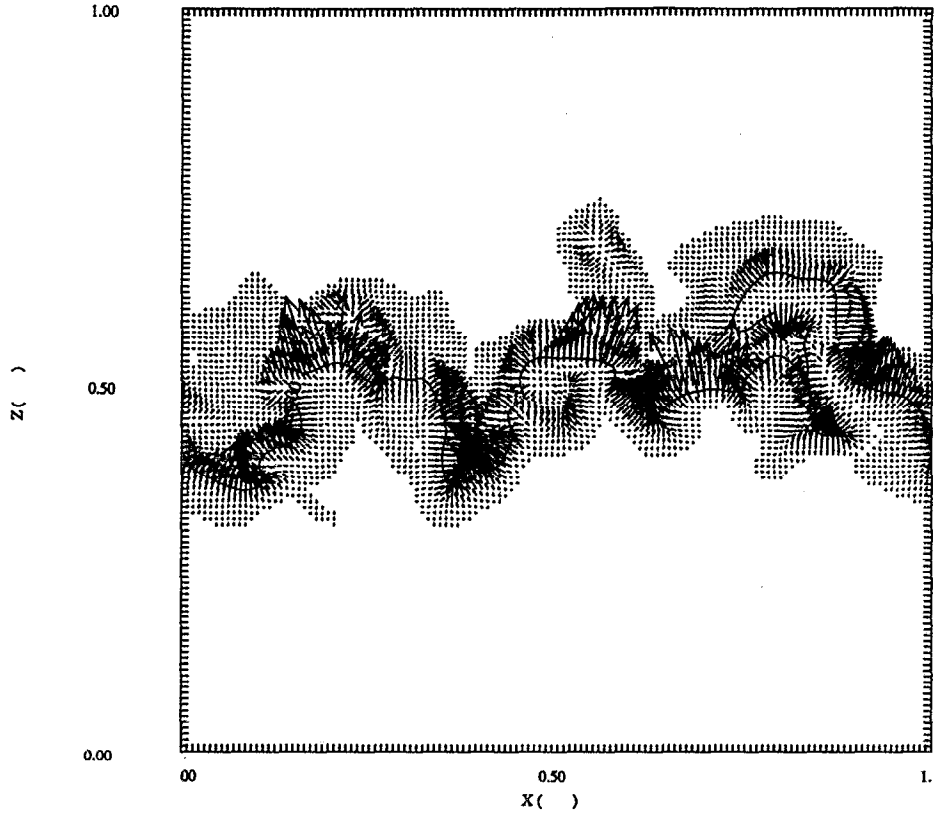

(a)

FIG. 21. Instantaneous scalar dissipation rate ϵ_F in a vertical (x-z) plane with isoscalar contour lines $F = 0.5$ at time $t = 6$ for (a) case IH (isotropic) and (b) case H ($St_0 = 1.0$).

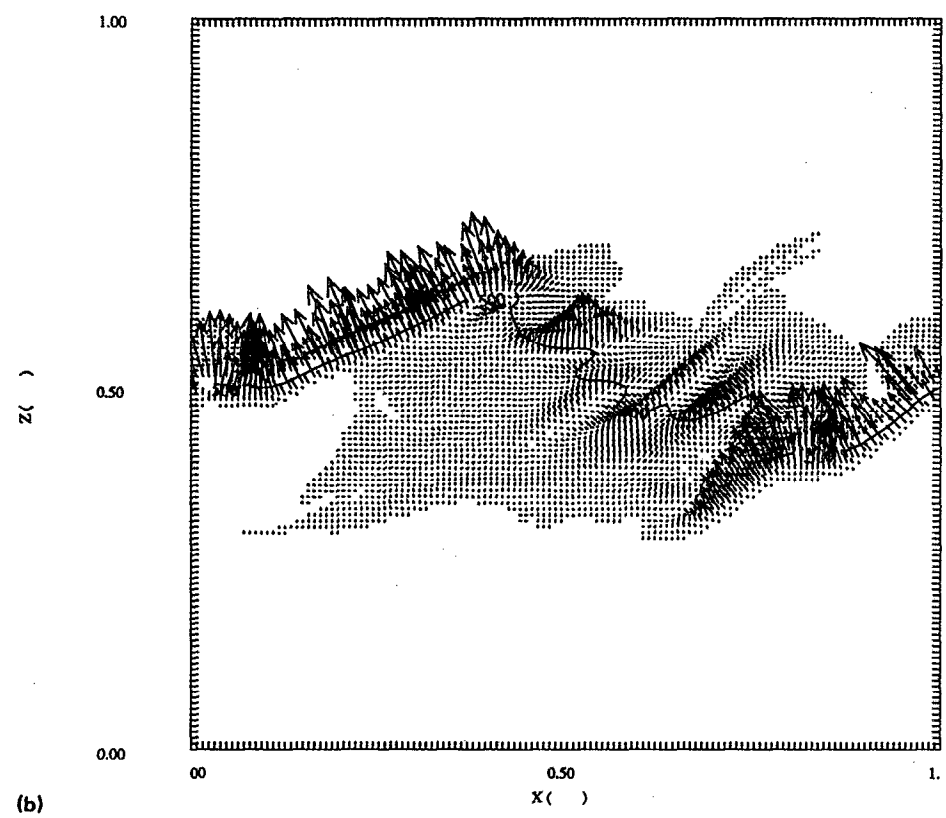

(b)

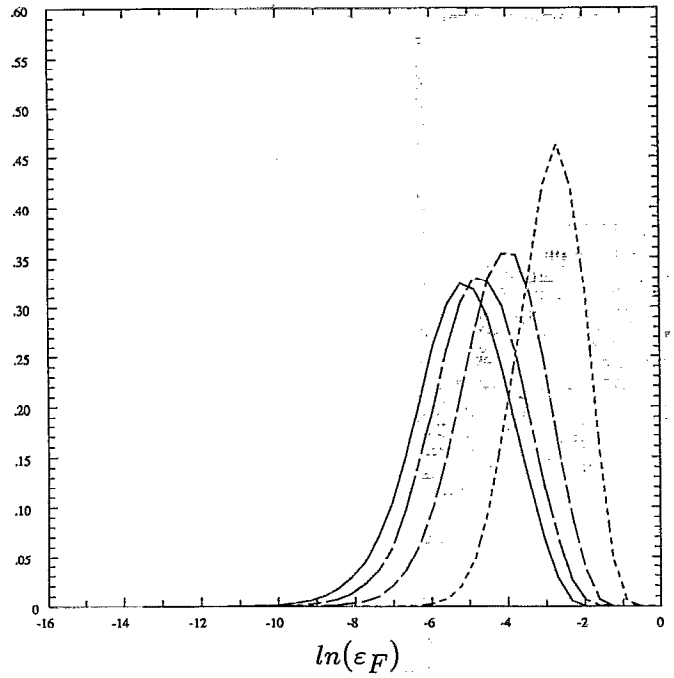

(a)

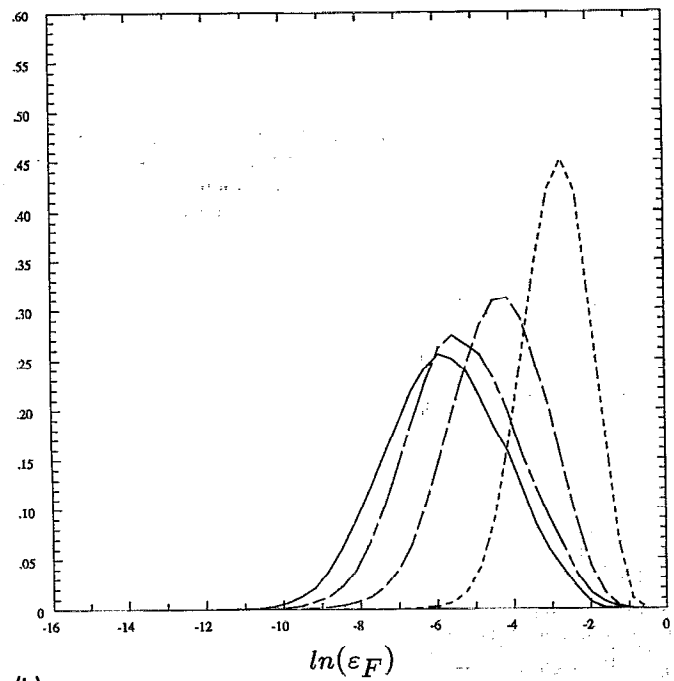

(b)

FIG. 22. Probability density function of logarithm of scalar dissipation rate (sample over $0.1<F<0.9$) for (a) case IH (isotropic) and (b) case H ($St_0 = 1.0$); $t = 2$ (----), $t = 4$ (– – –), $t = 6$ (— · —), and $t = 8$ (——).

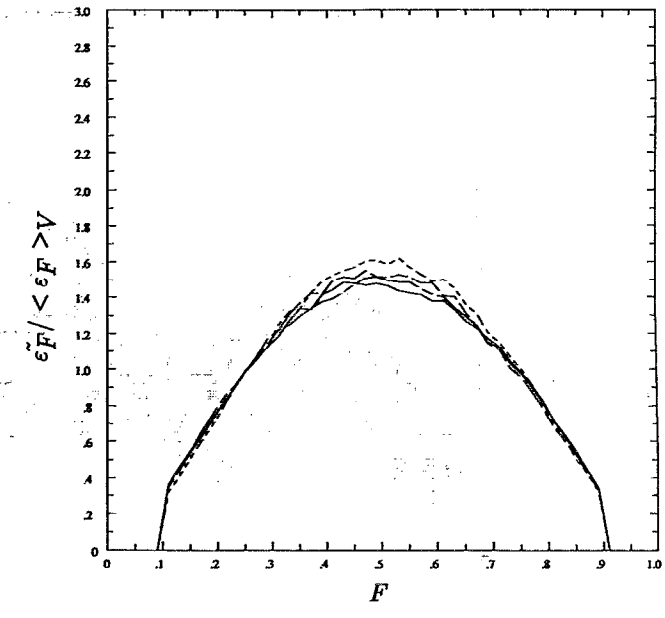

(a)

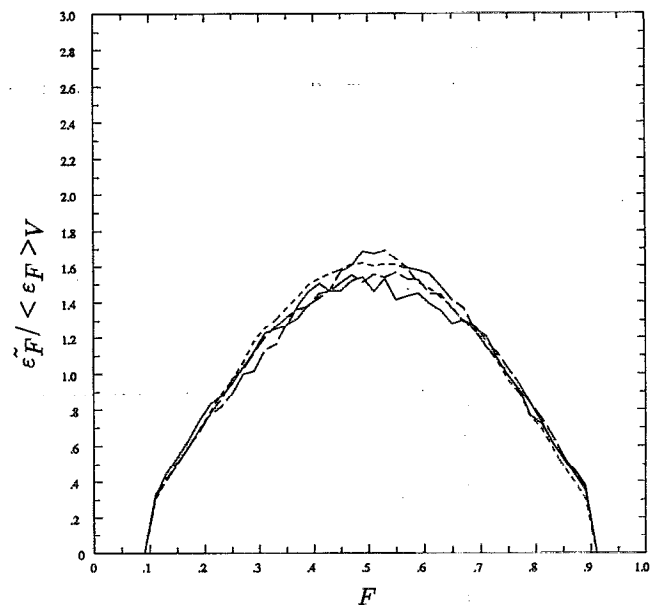

(b)

FIG. 23. Conditional expectation of scalar dissipation rate (sample over $0.1<F<0.9$) for (a) case IH (isotropic) and (b) and case H ($St_0 = 1.0$); $t = 2$ (----), $t = 4$ (– – –), $t = 6$ (— · —), and $t = 8$ (——).

pared with values for a normal distribution which are 0. and 3., respectively. The peak of the pdf's for both H and IH cases shift toward lower values of $\ln(\epsilon_F)$ as time increases, indicating a drop in $\langle \epsilon_F \rangle$ due to mixing. Figure 23 shows the conditional expectation of the scalar dissipation rate (conditioned on the value of F) $\tilde{\epsilon}_F$ normalized by the ensemble average of ϵ_F in the sample volume $\langle \epsilon_F \rangle_V$ for cases IH and H. A nearly parabolic shape remains throughout the development of the scalar mixing layer. This is characteristic of the mixing zone between two homogeneous regions of fluid.[33]

IV. CONCLUSIONS

Direct numerical simulation of an initial steplike scalar field subjected to homogeneous sheared turbulence has been performed and the results compared with those of the case of decaying isotropic turbulence. Statistics on the strain rate, vorticity, scalar gradient, and scalar dissipation rate were

obtained. Analysis of the flow field is consistent with previous studies[8,9,24] and suggests that turbulent flow consists of stretching vortex structures that generate higher strain rates in the normal plane. The structure of the vorticity field in isotropic turbulence tends to be sheetlike for moderate-valued vorticity and tubelike at high-valued vorticity.[11,12] In sheared turbulence, large-scale organized structures are present in the form of sheets and hairpins.

The strain rate and vorticity fields dominate the behavior of the scalar field and thus the reactive interface. The gradient of the conserved scalar tends to align itself with the axis of the most compressive strain rate and orthogonal to the local vorticity. The magnitude of the scalar gradient is directly influenced by the local strain rate while its orientation is controlled by the local vorticity. Because of the directional features of sheared turbulence, the orientation of the scalar gradient is more ordered than in isotropic turbulence. In addition, the magnitude of vorticity indirectly affects that of the scalar gradient through strain-rate amplification by vortex stretching. In both flows, regions of high scalar-gradient magnitude exist as sheets in the vicinity of sheetlike vortex structures of moderate to high vorticity. The sheetlike nature of the vortex structures appears to provide a locally unidirectional strain field that is capable of producing extended regions of high scalar gradient. This is of particular importance in reactive flows, where the most intense reactions will tend to occur where $(\nabla F)^2$ is high. Regions of intense reaction will therefore most likely exist as sheets, particularly in flows with mean shear where the well-correlated large-scale motion produces high $(\nabla F)^2$ sheets that are continuous over a greater spatial extent.

Influence of the fluid strain rate on $(\nabla F)^2$, and therefore ϵ_F, is indicated by the strain rate–scalar dissipation correlation coefficient Σ, which is independent of the scalar value and remains relatively constant in time. The statistical distribution of the scalar dissipation rate ϵ_F for an inhomogeneous scalar field exhibits a nearly lognormal distribution with a slight negative skewness for both isotropic and shear cases. The conditional expectation of the scalar dissipation $\tilde{\epsilon}_F$ remains parabolic for both decaying isotropic turbulence and shear flow.

ACKNOWLEDGMENTS

We would like to thank Dr. A. Schiano and E. Hood for their assistance in the three-dimensional graphics. Computations were performed on the Cray-2 (NAS) at the NASA Ames Research Center and the Cray Y-MP at the San Diego Supercomputer Center.

This work was also supported in part by the University of California—Irvine through an allocation of computer time on the Convex C240.

[1] S. P. Burke and T. E. W. Schumann, "Diffusion flames," Ind. Eng. Chem. **20**, 998 (1928).
[2] Y. B. Zeldovich, "On the theory of combustion in initially unmixed gases," Zh. Tekh. Fiz. **19**, 10 (1949) [English translation, NACA Tech. Memo. No. 1296 (1950)].
[3] A. M. Obukhov, "Struktura temperaturnovo polia v turbulentnom potoke," Izv. Akad. Nauk SSSR Ser. Geofiz. **13**, 77 (1949).
[4] S. Corrsin, "On the spectrum of isotropic temperature fluctuations in isotropic turbulence," J. Appl. Phys. **22**, 469 (1951).
[5] G. K. Batchelor, "Small-scale variation of convected quantities like temperature in turbulent fluid. Part 1. General discussion and the case of small conductivity," J. Fluid Mech. **5**, 113 (1959).
[6] C. H. Gibson, "Fine structure of scalar fields mixed by turbulence: I. Zero gradient points and minimal gradient surfaces," Phys. Fluids **11**, 2305 (1968).
[7] C. H. Gibson, W. T. Ashurst, and A. R. Kerstein, "Mixing of strongly diffusive passive scalars like temperature by turbulence," J. Fluid Mech. **194**, 261 (1988).
[8] R. M. Kerr, "Higher-order derivative correlations and the alignment of small-scale structures in isotropic numerical turbulence," J. Fluid Mech. **153**, 31 (1985).
[9] W. T. Ashurst, A. R. Kerstein, R. M. Kerr, and C. H. Gibson, "Alignment of vorticity and scalar gradient with strain rate in simulated Navier–Stokes turbulence," Phys. Fluids **30**, 2343 (1987).
[10] M. M. Rogers and P. Moin, "The structure of the vorticity field in homogeneous turbulent flows," J. Fluid Mech. **176**, 33 (1987).
[11] Z-S. She, E. Jackson, and S. A. Orszag, "Intermittent vortex structures in homogeneous isotropic turbulence," Nature **344**, 226 (1990).
[12] G. R. Ruetsch and M. R. Maxey, "Small-scale features of vorticity and passive scalar fields in homogeneous isotropic turbulence," Phys. Fluids A **3**, 1587 (1991).
[13] A. D. Leonard and J. C. Hill, "Direct numerical simulation of a homogeneous turbulent reacting flow," AIAA Paper No. AIAA-88-3624, 1988.
[14] K. K. Nomura and S. E. Elghobashi, "Direct simulation of an isothermal nonpremixed flame in homogeneous turbulent shear flow," AIAA Paper No. AIAA-90-0148, 1990.
[15] S. E. Elghobashi and K. K. Nomura, "Direct simulation of a passive diffusion flame in sheared and unsheared homogeneous turbulence," *Turbulent Shear Flows 7*, edited by W. C. Reynolds (Springer-Verlag, Berlin, 1991).
[16] A. D. Leonard and J. C. Hill, "Kinematics of the reaction zone in homogeneous turbulence," presented at the 12th Symposium on Turbulence, University of Missouri, Rolla, Missouri, 1990.
[17] S. E. Elghobashi, T. Gerz, and U. Schumann, "Direct simulation of the initial development and the homogeneous limit of the thermal mixing layer," Sixth Symposium on Turbulent Shear Flows, Toulouse, France, 1987, p. 511.
[18] U. Schumann and G. S. Patterson, "Numerical study of pressure and velocity fluctuations in nearly isotropic turbulence," J. Fluid Mech. **88**, 685 (1978).
[19] V. Eswaran and S. B. Pope, "An examination of forcing in direct numerical simulation of turbulence," Comput. Fluids **16**, 257 (1988).
[20] T. Gerz, U. Schumann, and S. E. Elghobashi, "Direct numerical simulation of stratified homogeneous turbulent shear flows," J. Fluid Mech. **200**, 563 (1989).
[21] S. Timoshenko and J. N. Goodier, "Theory of elasticity," *Engineering Societies Monographs* (McGraw-Hill, New York, 1951).
[22] R. Betchov, "An inequality concerning the production of vorticity in isotropic turbulence," J. Fluid Mech. **1**, 497 (1956).
[23] A. A. Townsend, *The Structure of Turbulent Shear Flow*, 2nd ed. (Cambridge U.P., Cambridge, 1976).
[24] R. M. Kerr, "Histograms of helicity and strain in numerical turbulence," Phys. Rev. Lett. **59**, 783 (1987).
[25] G. K. Batchelor, *The Theory of Homogeneous Turbulence* (Cambridge, U.P., Cambridge, 1959).
[26] P. Moin and J. Kim, "The structure of the vorticity field in turbulent channel flow. Part 1. Analysis of instantaneous fields and statistical correlations," J. Fluid Mech. **155**, 441 (1985).
[27] K. R. Sreenivasan, "Turbulence and the tube," Nature **344**, 192 (1990).
[28] S. Corrsin, "Remarks on turbulent heat transfer," *Proceedings of the Iowa Thermodynamics Symposium* (State University of Iowa, Iowa City, Iowa, 1953), pp. 5–30.
[29] R. W. Bilger, "Turbulent diffusion flames," Annu. Rev. Fluid Mech. **21**, 101 (1989).
[30] A. S. Gurvich and A. M. Yaglom, "Breakdown of eddies and probability distributions for small-scale turbulence," Phys. Fluids Suppl. **10**, S59 (1967).
[31] W. Y. Chen, "Lognormality of small-scale structure of turbulence," Phys. Fluids **14**, 1639 (1971).
[32] R. A. Antonia and K. R. Sreenivasan, "Log-normality of temperature dissipation in a turbulent boundary layer," Phys. Fluids **20**, 1800 (1977).
[33] V. Eswaran and S. B. Pope, "Direct numerical simulation of the turbulent mixing of a passive scalar," Phys. Fluids **31**, 506 (1988).